DEVELOPING FRAGILITY FUNCTIONS FOR MARINE VESSELS FROM FIELD SURVEY IN GUMBET BAY AFTER 20 JULY 2017 BODRUM-KOS TSUNAMI

A THESIS SUBMITTED TO
THE GRADUATE SCHOOL OF NATURAL AND APPLIED SCIENCES
OF
MIDDLE EAST TECHNICAL UNIVERSITY

BY

MERVE BILGIN

IN PARTIAL FULFILLMENT OF THE REQUIREMENTS
FOR
THE DEGREE OF MASTER OF SCIENCE
IN
CIVIL ENGINEERING

SEPTEMBER 2019

Approval of the thesis:

DEVELOPING FRAGILITY FUNCTIONS FOR MARINE VESSELS FROM FIELD SURVEY IN GUMBET BAY AFTER 20 JULY 2017 BODRUM-KOS TSUNAMI

submitted by **MERVE BILGIN** in partial fulfillment of the requirements for the degree of **Master of Science in Civil Engineering Department, Middle East Technical University** by,

Prof. Dr. Halil Kalıpçılar
Dean, Graduate School of **Natural and Applied Sciences** _____

Prof. Dr. Ahmet Türer
Head of Department, **Civil Engineering** _____

Prof. Dr. Ahmet Cevdet Yalçıner
Supervisor, **Civil Engineering, METU** _____

Examining Committee Members:

Assoc. Prof. Dr. Utku Kanoğlu
Aerospace Engineering, METU _____

Prof. Dr. Ahmet Cevdet Yalçıner
Civil Engineering, METU _____

Assist. Prof. Dr. Gülizar Özyurt Tarakcıoğlu
Civil Engineering, METU _____

Assist. Prof. Dr. Cüneyt Baykal
Civil Engineering, METU _____

Assist. Prof. Dr. Aslı Numanoğlu Genç
Civil Engineering, TED University _____

Date: 12.09.2019

I hereby declare that all information in this document has been obtained and presented in accordance with academic rules and ethical conduct. I also declare that, as required by these rules and conduct, I have fully cited and referenced all material and results that are not original to this work.

Name, Surname: Merve Bilgin

Signature:

ABSTRACT

DEVELOPING FRAGILITY FUNCTIONS FOR MARINE VESSELS FROM FIELD SURVEY IN GUMBET BAY AFTER 20 JULY 2017 BODRUM-KOS TSUNAMI

Bilgin, Merve
Master of Science, Civil Engineering
Supervisor: Prof. Dr. Ahmet Cevdet Yalçıner

September 2019, 88 pages

20 July, 2017 Bodrum-Kos earthquake occurred in Gokova Bay caused a tsunami and majority of the marine vessels have significantly been dragged by the tsunami. There were minor, moderate and major damages on the marine vessels in Gumbet Bay. The current velocities and water elevation changes caused by tsunami are computed from the mathematical model NAMI DANCE by applying the three different tsunami source models and the source which results in the most compatible results with the field survey observations is selected. Then, the damage on the boats are extracted from the field survey findings. A complete analysis of the damage distribution of the vessels is performed. The computed current velocities and water elevations as well as damage findings and vessel properties are used in developing tsunami fragility curves. The resulted fragility functions for the boat damage in Gumbet Bay are presented and discussed.

Keywords: Fragility Functions, Tsunami Simulation, Nami Dance, Marine Vessels, 2017 Bodrum-Kos Tsunami

ÖZ

20 TEMMUZ 2017 BODRUM-KOS TSUNAMI SONRASI GÜMBET KOYU SAHA ARAŞTIRMASINA GÖRE TEKNE HASAR FONKSYONLARI GELİŞTİRİLMESİ

Bilgin, Merve
Yüksek Lisans, İnşaat Mühendisliği
Tez Danışmanı: Prof. Dr. Ahmet Cevdet Yalçıner

Eylül 2019, 88 sayfa

20 Temmuz, 2017 tarihinde meydana gelen, Bodrum-Kos depremi nedeniyle oluşantsunami özellikle Gümbet koyunda deniz taşıtlarının büyük çoğunluğunun sürüklenmesine ve bir kısmının küçük, orta derece ve büyük düzeyde hasara uğramasına neden olmuştur. Tsunami ile oluşan akıntı hızları ve su seviyesi değişimleri, tsunami sayısal modeli NAMI DANCE kullanılarak hesaplanmıştır. Modelde üç farklı tsunami kaynağı kullanılmış, saha araştırması sonuçları ile en çok uygunluk gösteren tsunami kaynağı seçilerek bu çalışmada kullanılmıştır. Daha sonra, Gümbet koyu özelinde teknelerde oluşan hasar, yapılan saha araştırma sonuçları incelenerek analiz edilmiştir. Teknelerin elde edilen hasar dağılımları kullanılarak, oluşan hasar ile tekne özellikleri arasındaki ilişkilerin tam bir analizi yapılmıştır. Hesaplanan akıntı hızları ve su seviyesi değişimleri ile hasar dağılımları ve tekne özellikleri kullanılarakGümbet koyundaki tekneler özelinde tsunami kırılganlık fonksiyonları geliştirilmiş, sonuçlar tartışılarak sunulmuştur.

Anahtar Kelimeler: Kırılganlık Fonksiyonu, Tsunami Simulasyonu, Nami Dance, Deniz Taşıtları, 2017 Bodrum-Kos Tsunami

To my beloved family,

ACKNOWLEDGEMENTS

I cannot find enough words to express my gratitude to Prof. Dr. Ahmet Cevdet Yalçıner for his support and guidance. This study was only possible because he believed in me. He is a ray of sunshine that enlighten many lives he touched including me and will always be the most influential person in my life.

I also would like to thank the examining committee members Utku Kanoğlu, Gülizar Özyurt Tarakcıoğlu, Cüneyt Baykal and Aslı Numanaoğlu Genç for their invaluable advice on my thesis.

I would like to express my sincere thanks to Gözde Güney Doğan whom I had a chance to know better during the last stages of my study, for her invaluable support during the long study nights.

I would like to thank my dearest friend Ezgi Budak from the bottom of my heart for being the soothing voice at the end of the phone. She encouraged me with her words and were there for me. I would like to thank Hüseyin Çötel for enhancing my study with his advice. I also would like to thank Barış Akdeniz, Sinan Arslan, Salih Alaca, Orhan Ahmet Çelik, Oğuz Bolat and Can Değerli for making my undergraduate memories full of warmth and laughter.

I would like to thank my colleagues Merve Sinem Koç, Mehtap Atlı and İrem Birant for their friendship. My life in İstanbul is better because I have them.

I would like to thank my sister Salma Moustafa for giving me courage and inspiration during many hours of conversations. Despite distances between our cities, I knew that our hearts are never apart.

My biggest gratitude belongs to my family for their endless understanding and love. They have been always there as continual source of support. They made me who I am and I want to dedicate this thesis to them.

TABLE OF CONTENTS

LIST OF TABLES

TABLES

LIST OF FIGURES

FIGURES

CHAPTER 1

INTRODUCTION

Throughout the history coastal cities often carried great importance for their region by being an irreplaceable source of food, center of trade and lately, heart of the tourism and energy resources. Due to their unique terrain, coastal areas and coastal utilities unfortunately be the target of not only merchants and fishers but also natural hazards, and for this study most importantly tsunamis.

Interational Tsunami Information Center (ITIC) of United Nations Educational, Scientific and Cultural Organization (UNESCO) describes tsunamis as an impulsive wave or series of waves generating from movement of water body by the disruptions of the state of sea floor. This disturbance can be caused by submarine activities as volcanic eruptions, landslides and mainly earthquakes. Though the accurate translation of the term "Tsunami" is rather a simple and neutral Japanese word which means "harbor wave" the aftermath of such events are rarely ever as banal or harmless. Tsunamis are affecting the countries by causing vast number of casualties, destroying buildings and marine activities resulting a major blow to the economy.

On July 21, 2017 an earthquake occurred in Gokova Bay with a moment magnitude of Mw=6.6 (Ml= 6.2). The tsunami's aftermath is inspected at the southern face of Bodrum peninsula by a field survey team. The tsunami survey report estimated that the tsunami washed away most of the boats in the bay and dragged some of them to the easternmost part of Gumbet bay. There were more than 30 damaged boats while the number of submerged ones was given as 10 at this position (Yalçıner et al., 2017).

The event once more pointed out that East Mediterranean coasts has a considerable damage potential on the coastal utilities and maritime properties against the tsunamis. Therefore, a need of a detailed analysis of the tsunami damage at the mentioned region

is urged to help improving risk mitigation policies. As a result, a study on the fragility and vulnerability of marine vessels due to tsunami at the Gumbet Bay is decided to be conducted.

This research proposes to implement fragility curves to describe the damage probability of marine vessels in Gumbet Bay. Analyzing the impact of tsunami parameters and the marine vessels properties on the intensity of damage, it is aimed to find a proper statistical method that can express such relationship with minimum uncertainty. An insight to the work scheme used and the summary of the following chapters are given in the following.

In Chapter 2, the literature survey of the historical studies and recent developments on the numerical tsunami modeling is given. In addition, to underline the tsunami damage potential of the region, information about historical tsunamis in the Aegean Sea are referred. Lastly, the appliances of the fragility curves in the tsunami field and related studies are given.

Information about the tsunamigenic earthquake and findings of the tsunami field survey are summarized in Chapter 3. The required information to choose complementary data points to help better analysis of the fragility function are obtained by the examination of field reports.

In Chapter 4, tsunami parameters of 2017 Bodrum-Kos tsunami are numerically modeled with NAMI DANCE tsunami simulation tool using accurate bathymetric and topographic information for the Bodrum-Kos domain and Gumbet domain. 3 different source models are compared according to their performance of satisfying damage criteria. To process output of the simulations and create visuals, Surfer 13 and Grapher 12 software are used. The resulting time histories of tsunami parameters are given for water elevation and current velocity. These tsunami parameters used as tsunami intensity measures of fragility functions for the following analyses.

After then, the dataset is prepared in Chapter 5 to conduct vulnerability analysis. The number of vessels at certain berthing places are determined using satellite images from

Google Earth and verified with the observations. Vessel properties such as vessel length, production material and tonnage are also documented. Survey photographs of the berthing places are examined and the vessels are categorized as survived, washed away or with an explanatory damage quantity in matching the classification of Suppasri et al., (2014). A preliminary vulnerability analysis conducted and the damage ratios defined by (Aketa, Yano, Mizuno, Sato, & Terauchi, 1994) are computed.

In Chapter 6, statistical analysis is done to obtain fragility curves. First, probability of damage for each range of tsunami intensity measure is calculated using the definition of probability of occurrence. Then, a number of regression models are compared to find the most suitable model to dataset. To compute errors of the models and obtain the best fit, machine learning tool library in MATLAB is used. The results of linear regression model using least square method is compared with general linear model that uses maximum likelihood estimation. After choosing the most suitable fit, fragility curves of damage levels are obtained for water elevation and current velocity based on vessel material and weight.

CHAPTER 2

LITERATURE SURVEY

2.1. Tsunami Modeling

Numerical models provide us calculation of tsunami parameters to open a window to see a better view of the relationship between these parameters and other variables such as bathymetry, topography and characteristics of the tsunami source. They aim to predict an accurate model for tsunami generation, propagation and inundation in the possible shortest duration to let academic studies and operational issues to be conducted as sufficient as possible.

The modelling process often involves three stages. First of all, the most feasible bathymetry and topography maps are obtained for a certain domain. The computational models implementing shallow water theory such as Imamura (1996) create solutions in shorter times and often preferred. However, for more detailed studies they require maps with finer resolutions. Experiment on tsunami models to compute wave characteristics in harbors state that to come up with accurate results for this kind of detailed analyses, the grid size of the input data needs to be at 10 m or less (Admire et al., 2014; Uslu, Admire, & Dengler, 2013).

Later, the possible sources that generated the tsunami have been compared to identify the most authentic source characteristics. Lastly, based on the features of the inputs discussed in the first two steps, the most suitable computation method is decided and applied. Basic equations used for these numerical simulations have different approaches. For example, a Boussinesq model implements dispersive equations while nonlinear shallow water theory allows the implementation of nondispersive formula for solutions.

There are considerable number of computative tsunami models available in the field(Lynett et al., 2017). Descriptions and principals of some of these numerical models which have already been applied in such kind of studies are as follows;

TUNAMI-N2 defines the tsunami source parameters by using seismic rupture characteristics and solves nonlinear shallow water equations and compute/analyze generation, propagation and coastal amplification of tsunamis due to the inputted rupture parameters and or tsunami sources. The model computes all necessary parameters to analyze behavior of tsunami in shallow and inundation zones (Imamura, Yalçıner, & Özyurt, 2006).

COMCOT is developed by Cornell University (USA). Shallow water wave equations, finite difference method and leap-frog scheme method are used in the model. Selection of coordinate system (cartesian or spherical) is allowed and nested grids are used in the model. Submarine landslide, seismic fault and any surface deformation can be used as the source of tsunami generation. The model is efficient and accurate. Selection of tsunami generation mechanism is an advantageous feature for the model. The model is used for modeling of wave generation, propagation, run-up and inundation.

MOST is created by Titov and Synolakis, (1998) and has been developed over several decades with multiple co-authors (Titov, Kânoğlu, & Synolakis, 2016). The MOST model provides solutions to the NSW equations, including generation, propagation and inundation onto dry land (e.g. Gica et al., 2008; Wei et al., 2008)The model uses an explicit scheme to discretize the NSW equations, using an algorithm based on the method of fractional steps (Durran, 1999; Yanenko, 1971). Complied executables for the model are freely distributable, but the source code is proprietary.

NAMI DANCE implements NSW equations with a bottom friction term and solves using the Leap-Frog numerical scheme (Imamura, 1989; Shuto et al., 1990). The model takes an input tsunami source from either a defined rupture, predetermined wave form, or time history of water surface fluctuation at a grid boundary and computes propagation, coastal amplification, and inundation (e.g. Ozer Sozdinler et

al., 2015, Dilmen et al., 2015). Complied executables for the model are freely distributable, but the source code is proprietary.

2.1.1. NAMI DANCE

NAMI DANCE is a computational tool designed for modeling and visualization of tsunamis simulations. It is developed using C++ programming language with a similar computational approach to another model TUNAMI-N2 (Goto & Ogawa, 1997; Imamura, 1989; Imamura et al., 2006; Shuto, Goto, & Imamura, 1990) by following leap frog scheme numerical solution procedures(Zaytsev, Yalçıner, Chernov, Pelinovsky, & Kurkin, 2016).

Scientist contributed to development of NAMI DANCE are Andrey Zaytsev, Ahmet Cevdet Yalciner, Anton Chernov, Efim Pelinovsky and Andrey Kurkin from different organizations; Middle East Technical University Civil Engineering Department Ocean Engineering Research Center, Turkey; Special Research Bureau for Automation of Marine Researches and Far Eastern Branch of Russian Academy of Sciences, Russia. It is improved further recently to perform runs with Graphics Processing Unit (GPU) by Bora Yalciner, Andrey Zaytsev, Ahmet Cevdet Yalciner, Efim Pelinovsky and Andrey Kurkin.

NAMI DANCE outputs tsunami parameters for any requested point in the domain. In addition, it performs many computations including; determination of tsunami source from both rupture characteristics and a certain waveform input, wave propagation, tsunami arrival duration, inundation, coastal amplification, water surface elevations and time histories of water surface fluctuations, distribution and directions of the current velocity vectors along the domain. Moreover, it creates 3D sea state plots and animates tsunami propagation (Yalçıner, Synolakis, González, & Kanoglu, 2007).

NAMI DANCE provides users an option to choose between two different coordinate system such as spherical or Cartesian and also two equation types of linear or nonlinear shallow water equations. It can create the tsunami initial wave either from tsunamigenic rupture parameters or an initial water surface disturbance area defined

by the user. Input can be given to the program as a static source initial wave or a dynamic source initial wave such as time history of water elevation.

Great amount of studies has been performed by NAMI DANCE for different tsunami events. Studies by Yalçıner et al., (2001, 2002, 2003, 2004), Zahibo et al., (2003) proved the reliability of the NAMI DANCE model for several times (Yalciner et al., 2014; Yalciner & Pelinovsky, 2007; Yalçıner, Özer, Karakuş, Zaytsev, & Guler, 2010; Zaytsev, Kostenko, Kurkin, Pelinovsky, & Yalçıner, 2016; Zaytsev et al., 2008). Moreover, UNESCO recommends NAMI DANCE for tsunami modeling.

2.1.2. Computational Background

NAMI DANCE solves Nonlinear Shallow Water Equations (NSWE) since it provides a convenient run time and relatively reasonable memory usage within acceptable error limits. Shallow water equations are obtained by Navier-Stokes Equations applying conservation of mass and momentum in two-dimensional unsteady solution.

According to Shallow Water Theory, the vertical acceleration component of the water particles in z direction is very small compared to gravitational acceleration component (in x and y direction) and can be neglected. Therefore, there is no impact of the vertical motion of the water particles in pressure distribution.

At the free surface, the surface tension force between air and water is neglected and this is called the dynamic boundary condition. In addition, the water particle on the free surface assumed to keep its position throughout the motion which referred as kinematic boundary condition.

In addition, apart from run-up calculations, it is assumed that the bottom friction governs over the horizontal turbulence for tsunami waves propagating in shallow waters. (Imamura et al., 2006).

After the applications of boundary conditions at the sea surface and the bottom to two dimensional NSWE, (Equations 4.1, 4.2, 4.3) the final fundamental equations for NAMI DANCE are obtained with dispersion term.

$$\frac{\partial \eta}{\partial t} + \frac{\partial M}{\partial x} + \frac{\partial N}{\partial y} = 0 \quad [4.1]$$

$$\frac{\partial M}{\partial t} + \frac{\partial}{\partial x}\left(\frac{M^2}{d}\right) + \frac{\partial}{\partial y}\left(\frac{MN}{d}\right) = gd\frac{\partial \eta}{\partial x} + \frac{\tau_x}{\rho} = \frac{\partial \psi}{\partial x} \quad [4.2]$$

$$\frac{\partial N}{\partial t} + \frac{\partial}{\partial x}\left(\frac{MN}{d}\right) + \frac{\partial}{\partial y}\left(\frac{N^2}{d}\right) = gd\frac{\partial \eta}{\partial y} + \frac{\tau_y}{\rho} = \frac{\partial \psi}{\partial y} \quad [4.3]$$

In these equations, x and y are the axes of Cartesian coordinate, t is time, η is water surface elevation above still water level up to free surface. The total water depth is D=d+η , g is gravitational acceleration, ρ is the water density, τ_x and τ_y are the bottom shear stress in x and y directions.

The discharge fluxes in the x and y directions, M and N are given below

$$M = \int_{-h}^{\eta} udz = u(d+\eta) = ud, \quad N = \int_{-h}^{\eta} vdz = v(d+\eta) = vd \quad [4.4]$$

u and v represents current velocities in x and y directions respectively.

The bottom shear stresses with bottom friction, f is given in the equations 4.5, 4.6

$$\frac{\tau_x}{\rho} = \frac{fn^2}{D^{7/3}} M\sqrt{M^2+N^2} \quad [4.5]$$

$$\frac{\tau_y}{\rho} = \frac{fn^2}{D^{7/3}} N\sqrt{M^2+N^2} \quad [4.6]$$

n is Manning's coefficient

$$n = \sqrt{\frac{fD^{1/3}}{2g}} \quad [4.7]$$

Finally, the dispersion terms are defined in the equations given below:

$$\psi = \frac{h^2}{3}\left(\frac{\partial^2 u}{\partial x \partial t} + \frac{\partial^2 v}{\partial y \partial t}\right) \quad [4.8]$$

where h is water depth with respect to disturbed water level.

2.2. Historical Tsunamis in Aegean Sea

The coast of the Aegean Sea has suffered from numerous tsunamis in history due to earthquakes (Tselentis, Stavrakakis, Makropoulos, Latousakis, & Drakopoulos, 1988) since the region is tectonically active (McKenzie, 1972). According to many studies and historical records, most of the eastern Mediterranean tsunamis have affected the coastal settlements in along the Aegean Sea (Altinok, Alpar, Özer, & Aykurt, 2011; Altinok & Ersoy, 2000; Ambraseys, 1960, 1962; Antonopoulos, 1978; G.A. Papadopoulos & Chalkis, 1984; Gerassimos A. Papadopoulos, 1993; Papazachos, Koutitas, Hatzidimitriou, Karacostas, & Papaioannou, 1986; Poirier & Taher, 1980). Especially in the South Aegean (the region of this study is located) several tsunamis were reported in the last century or so (Ambraseys 1962; Papadopoulos and Chalkis 1984; Papadopoulos et al. 2007; Altinok et al., 2011; G. A. Papadopoulos, Daskalaki, Fokaefs, & Giraleas, 2007). One of the most destructive event is the 9 July 1956 Amorgos tsunami which was triggered by a Mw = 7.4 earthquake (Beisel et al., 2009; Cakir & Yalciner, 2002; Galanopoulos, 1957; E. A. Okal, Synolakis, Uslu, Kalligeris, & Voukouvalas, 2009; Gerassimos A. Papadopoulos & Pavlides, 1992; A. C. Yalciner, Kuran, Akyarli, & Imamura, 1995). Altinok (2011) which is a study on tsunami catalogue affecting Turkish coasts and surrounding regions reports 51 events in the Aegean Sea among 134 tsunamigenic events over a span of 3500 years.

Two recent events occurred in 2017 in Aegean Sea. One is the Lesvos earthquake with Mw=6.2 magnitude on 12th of June, 2017, 12:28 UTC, at a location between Lesvos island (Greece) and Karaburun Peninsula in İzmir, Turkey (Dogan et al, 2018). The other one is the Bodrum-Kos earthquake which can be considered as an important warning for the coastal communities in this region. Central Aegean with increasing seismic activity with the current events is one of the important tsunami source areas due to the location between the North Anatolian fault zone in the North, and the Hellenic Arc in the South (Altinok, Alpar, Özer, & Gazioglu, 2005).

After the tsunamigenic Bodrum-Kos earthquake of June 20, 2017, many researchers studied the fault mechanisms, possible source parameters and the effects of the devastating tsunami.

This new event provided the possibility to have new insights about the tsunami damage potential of such events occurring in Aegean Sea. Thus, it is important to investigate the event from as many perspectives as possible.

2.3. Vulnerability Analyses and Fragility Functions

Fragility curves have been used as a method for loss estimation in many fields. However, for the purpose of tsunami damage estimation, the term "tsunami fragility" is firstly introduced by Koshimura et al., (2009). The early applications of the term were mainly focusing on describing the structure damage and fatality potential of a tsunami.

Suppasri et al., (2011) conducted a vulnerability study and created fragility curves for structures affected by 2004 Indian Ocean Tsunami. To describe the structural fragility against the risk of a tsunami, the study applied the concept of "tsunami fragility curves" developed using observation of satellite imagery before and after the incident. Based on the roof condition, the status of the building damage was determined. They developed a tsunami model focusing on inundation to replicate the tsunami characteristic of the event. The fragility function described by normal and log-normal curves. The least square fitting applied to data to of buildings with their respective construction material.

After 2011 Great East Japan Earthquake and Tsunami, East coast of Japan was devastated by the subsequent tsunami. Following the disastrous event, implementation of fragility functions in tsunami damage estimation has been improved by many studies to better understanding the risk potential and better preparation for the future.

Suppasri et al., (2012) has adopted a fragility curve approach for structures in Sendai and Ishinomaki Plains to reveal devastating impact of the incident. A field survey

conducted immediately following to assess the inundation depth and examine the damaged buildings. 4 level damage classification (minor, moderate, major and complete) is used to describe the level of damage on mostly wooden structures. The inundation depth and damage levels are correlated to develop the tsunami fragility curves. The corresponding damage levels for tsunami inundation depths considered minor between 2.5 and 3 m; moderate between 3–4 m; major between 4 and 4.5 m and complete if depth is bigger than 4.5 m. This classification resulted from the developed fragility curves for damages with a 50% chance of occurring threshold. The fragility curve showed also that the wooden structures in the site performed better than other wooden structures that were hit in the past by other tsunamis in other coasts. To elaborate further, the damage to the wooden structure increases when the inundation depth reaches and pass 3m, collapsing happens when inundation is greater than 4 m. On the other hand, wooden houses in the past tsunamis resist just up to 1 or 2 m. In addition, the study showed wooden walls have a low resistance when the tsunami hits in comparison with brick walls.

The loss function studies mentioned above were more concerned with recovery and reconstruction of the human casualties and destruction of building and infrastructure. On the other hand, there were a lack of information regarding the loss of marine crafts tough it is a very critical downturn for economies relying on coastal activities.

Suppasri et al., (2014) developed a loss function for damage on small marine vessels and involved the data collection of great amount of small sea crafts that hit in 2011 by the Great East Japan tsunami with the respective motor type, tonnage and distance to tsunami source. Maximum water elevation of the tsunami and velocity of flow were the tsunami parameters used as the second variable. They used methods of Aketa et al. (1994) for calculation of the damage ratio. Later they developed the loss function through linear regression analysis on these two variables with log-normal distribution. The results show that the damage probability grew remarkably if the tsunami elevation crossed 2 m or if the velocity of the current reached bigger values than 1 m/s. They reported the vessels weighing more than 5 tons experienced less damage. The vessels

near to tsunami get more damage as they collided with bigger tsunamis with less arrival times which allows limited time to flee.

Muhari et al., (2015) formed an updated loss function that describes the relation between tsunami parameters and the potential level of loss observed on marine craft. They collected the information from the southern part of Honshu Island to compute tsunami characteristics with a numerical model. They extracted the data for water elevation and flow velocity in the form of spatial and time series and implemented advanced statistical methods in order to come up with the most accurate dataset. To enable simultaneous application of different variables on loss function they implemented ordinal regression analysis on the data. The most prominent characteristic of this function is the capacity to bring together the essential determinants that affect the damage probability.

The latter applications of tsunami fragility have started to cover damage estimation of marine life since the environmental concerns reached its maximum. In this regard, Suppasri et al., (2018), studied the available data of two sites that were affected when the 2011 tsunami hit Japan focusing on marine ecosystems of aquaculture rafts and eelgrass. For the first part of their work, the tsunami in 2011 was modelled to replicate the same characteristic that affected their target regions. Later, the damages were examined with the help of pre and post 2011 tsunami satellite imagery of the aquaculture raft and eelgrass by inspection and binarization. After all, losses were computed to work out the fragility function analyzing the correlation of computed tsunami parameters with the calculated damage. The outcome of the statistical analysis was used to produce the fragility functions for Mangkuura Lake, where the main cause of the damage was the flow velocity rather than the wave amplitude. For instance, equality could be found between the 0.9 damage and the maximum flow velocities of 1.3 m/s (aquaculture raft) and 3.0 m/s (eelgrass).

After all, it can be said that the fragility curve is highly essential for the loss estimation and reconstruction as well as for future city planning and risk assessment and

management. Thus, developing damage estimation systems by improving fragility functions is critical and should be considered as a forward step in planning mitigation strategies.

2.4. SHAP (Shapley Additive explanation) Values

In the case of creating fragility curves with small set of data, understanding the nature of variables may help to explain why the statistical models used made certain predictions. Fragility curves are developed to predict damage for a given tsunami intensity measure and improve risk mitigation strategies. Thus, before acting based of the fragility curve obtained by a specific statistical model, it is more crucial to comprehend behavior of the dataset and interpreting it. However, the highest accuracy for datasets is often achieved by complex models that are hard to interpret. Therefore, scientist started to refer this gap between the accuracy and interpretability of statistical methods (Ribeiro, Singh, & Guestrin, 2016) as the machine learning tools become more and more complex.

In response, various methods have recently been proposed to help users interpret the predictions of models. The Shapley value has become favored method to interpret the prediction of a machine learning model in the input dataset, by its base features. The Shapley value is known to be the unique method that satisfies certain desirable properties. In contrary, there are many ways to apply the Shapley value that differ in how they reference the model, the training data, and the explanation context. Therefore, it is not unclear how these methods are related and when one method is preferable over another (Lundberg & Lee, 2017).

To overcome this challenge in the model interpretation we used a recently proposed method by Lundberg & Lee, (2017) that unifies six existing methods; SHAP (SHapley Additive exPlanations). SHAP is easy to understand since it assigns each feature in the dataset an importance value for prediction (damage level for our case) and shows better consistency with human intuition than previous approaches (Lundberg & Lee, 2017).

After it proposal SHAP method used in many studies in different fields from medical to transport engineering and it is verified by tests. (Lundberg & Lee, 2017; Hathaway et al., 2019; Pianpanit, Lolak, Sawangjai, Ditthapron, & Marukatat, 2019; Spadon, Carvalho, Rodrigues-Jr, & Alves, 2019)

CHAPTER 3

THE TSUNAMI AND THE FIELD SURVEY

3.1. The Bodrum-Kos Earthquake and Tsunami of July, 20 2017

On July 20, 2017 at 22:31 UTC (21 July 2017 at local time 01:31) a shallow earthquake happened in Gökova Bay. While more than 200 people injured in Bodrum city and Kos island, there were 2 casualties in the Kos island due to earthquake.(Kitsantonis, 2017; Smith & Rourke, 2017). The earthquake also caused property damage, including the tsunami damage along the coasts of Bodrum and Kos island (Dogan et al., 2019; Yalçıner et al., 2017).

The epicenter coordinates of the earthquake were given as 36.9620 North and 27.4053 East by Kandilli Observatory and Earthquake Research Institute (KOERI, 2017). The epicenter is given as about 12km eastnortheast of Kos, Greece and 8 km southsouthwest of Bodrum, Turkey. The moment magnitude of the earthquake was Mw=6.6 (Ml= 6.2) and the depth was 6 km according to KOERI. There were 1369 aftershocks recorded by AFAD (Disaster and Emergency Management Presidency Earthquake Department), (2017) , with magnitude range 1.0- 5.0 within the first five days after the earthquake. Figure 3.1 presents the location and focal mechanism solution of the mainshock and aftershocks taken from KOERI which reveal that the earthquake occurred with a normal faulting.

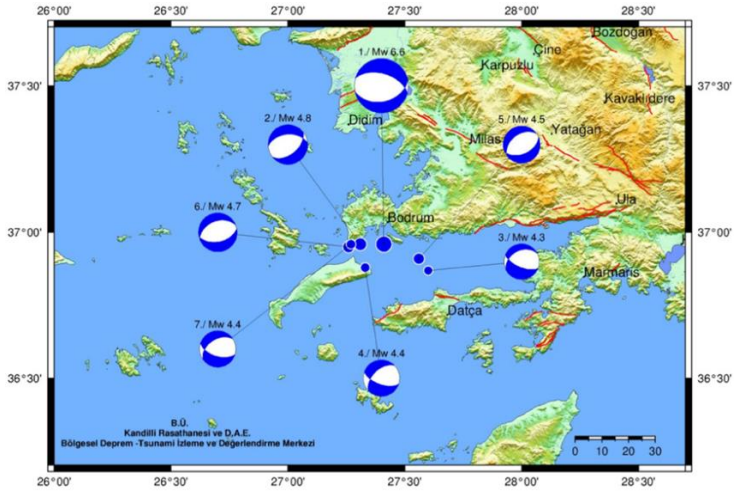

Figure 3.1. The image from KOERI showing the main shock and aftershocks (Yalciner et al. 2017)

As shown by the first intensity maps created by ELER (Earthquake Loss Estimation Routine) of KOERI, the intensity of the earthquake is level VII for Bodrum. This estimation means that the shaking felt by people was very strong while the damage potential of the earthquake was moderate. For Kos Island, Bodrum Peninsula and North of Datca Peninsula, this level was found as VI which indicates shaking was felt strongly but the damage potential was light. The earthquake intensity maps of the corresponding locations are taken from the KOERI (ELER) website and given in Figure 3.2.

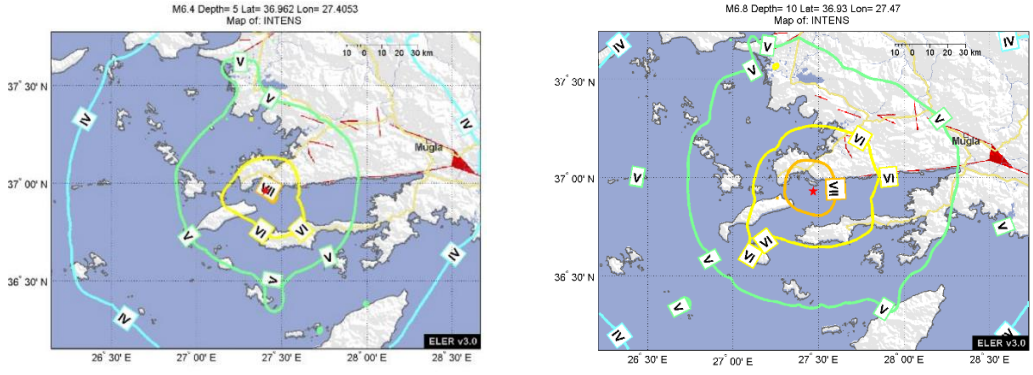

Figure 3.2. Earthquake Intensity Map produced by ELER (KOERI) for magnitudes a) M6.4; b) M6.8

There are many studies in literature that discuss the seismicity and the fault characteristics of the earthquake (Batıgün, Yolsal-Çevikbilen, & Taymaz, 2018; Kiratzi & Koskosidi, 2018; Papadopoulos et al., 2019).

The tsunami caused by the earthquake was recorded with a tide gauge located in Bodrum. The calibration of the gauge data and the analysis of the time series are done by Dogan et al., (2019) and Yalçıner et al., (2017) and the records are found reliable. The measurement of the tide gauge is also given in Figure 3.3.

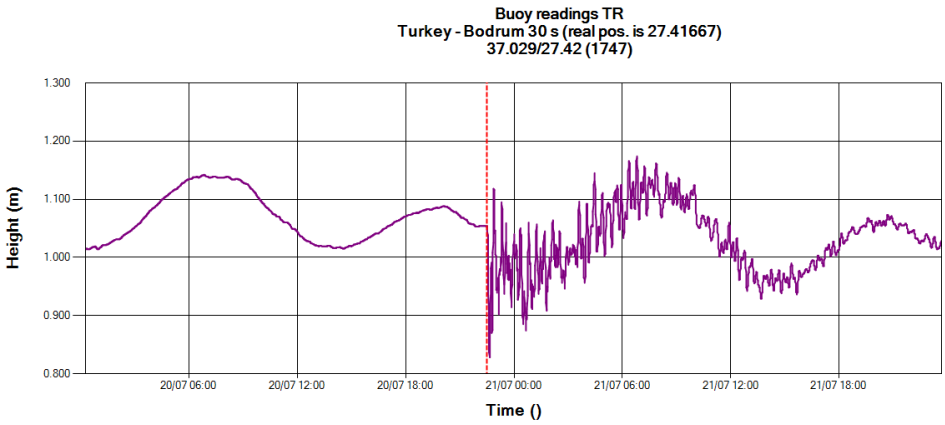

Figure 3.3. Sea Level Measurement of Tide Gauge in Bodrum (Yalciner et al. 2017)

3.2. Post-Tsunami Field Survey

The day after the earthquake, a research team from METU and KOERI in collaboration with Turkish Chamber of Civil Engineers (TCCE) held a tsunami field survey along the south coast of Bodrum Peninsula. Fishermen, visitors and other locals inquired to describe their observations. In this section the data and information from the tsunami survey reports (Dogan et al., 2019; Yalçıner et al., 2017) are summarized by focusing on the observed tsunami parameters and damages in Gumbet Bay. In addition, some of the observations will be stated to validate numerical tsunami model

in the following chapter. More information about the tsunami survey is provided in these references.

According to field survey studies (Dogan et al., 2019; Yalçıner et al., 2017), eyewitnesses in Gumbet Bay stated that, after the earthquake the water levels decreased for 5 minutes and then the first wave arrived after 12-13 minutes. In addition, the workers of Municipality café that located in the easternmost part of the Gumbet Bay (27.408503E 37.029732N) reported a roughly 20 m of inundation through the stream bed near the cafe. 12 of the parked cars near the shoreline had been dragged towards the concrete bed of dry stream and have been found at the same point (37.031137N 27.406882E) in the old stream bed. Besides, the workers of a sea front restaurant stated that the sea withdrawal and advancing continued with successive waves for three hours after the earthquake. The photograph in Figure 3.4 (a), taken by an eyewitness 3 hours after the earthquake around sunset, shows the significant sea withdrawal. In addition, about 6 hours after the earthquake (the next morning), 2 m of vertical decrease in the water level have been witnessed. Dead fishes and rare insects were found all along the coastline, but more accumulated around the stream bed.

The report also mentions that there were many cars parked over the bed of a stream that dried in summer. The stream was being used as a pathway bay the cars. The width of the pathway was measured to be 3.3 m and 5.7 m including the side walls. The waves mainly penetrated through this path in the old stream bed and inundated almost 100 m into the land (Figure 3.4 (b)). Flow depth reached up to 1 m in the stream bed. Security camera footage of a hotel at east end of the bay reveals that, sea level decreased at first 5 minutes after the earthquake and in 13 minutes inundation reached to 60 m. It is recorded that the current velocity was high and the flow depth reached up to 50-60cm.

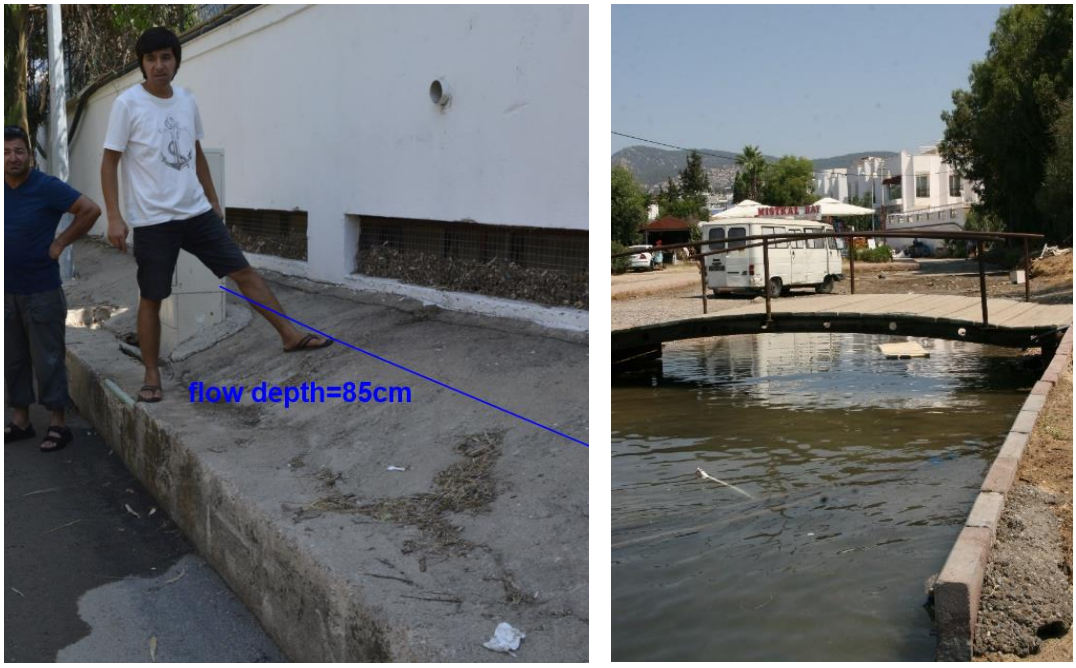

Figure 3.4. (a) Eyewitness showing the flow depth by his foot (37.031412N, 27.406703E), (b) the channel the tsunami inundated through

There were berthing places on the shallow water of the eastern shores of Gumbet bay where small boats moored (27.407621E, 37.037478N). The boats were flown by tsunami waves and carried in the direction of deep sea. The approximate coordinate of the location they found together is 27.405029 East, 37.0281.33 North of the bay. There were more than 30 damaged boats while the number of submerged ones was around 10 at in this position. At three points a very heavy vortex is witnessed by the seamen. Estimated coordinates of this points are given in the field survey report (Yalçıner et al., 2017) as follows; i) 27.405029E, 37.0281.33N; ii) 27.400399E, 32.029001N; iii) 27.403934E, 37.030043N.

After the examination of tsunami survey reports, according to given information, the eastern coast of the Gumbet Bay is selected as the area of interest to conduct fragility analysis on marine vessels. Moreover, locations of points that provide precise information on the tsunami parameters are determined by the help of witnesses reports

or camera footage. These points are considered as convenient gauge points to validate numerical tsunami model and used in the Chapter 4.

CHAPTER 4

NUMERICAL MODELLING AND SIMULATIONS

According to the field survey observations (Yalciner et al., 2017 and Dogan et al., 2019), it is clearly observed that Gumbet Bay is the most suitable region for investigation of the loss function due to tsunami action. Because it was the most hit region by the tsunami waves.

Tsunami currents and water elevations are accepted as damaging components of tsunami inundation (Lynett el al., 2014). However, for structural fragility, the significance of current velocity of the tsunami to structural damage often discussed and compared with inundation (De Risi et al., 2017; Song et al., 2017). On the other hand, according to field survey observations of Okal et al., (2006a, 2006b, 2006c) and the study of Lynett et al., (2012) tsunami surges causing damage at maritime facilities are not necessarily causing inundation. Lynett at al., (2014) states that tsunami parameters responsible for the ship damage can be considered independent from inundation. Therefore, the spatial and temporal change of tsunami parameters computed in Gumbet Bay are selected as water level and current speed in this study.

The tsunami generated by the Bodrum-Kos Earthquake is simulated by the tsunami numerical model NAMI DANCE. In order to perform accurate tsunami numerical modeling, the bathymetry and topography data should be in the highest resolution and the tsunami generation mechanism should be defined properly. For this reason, detailed data from different data sources are obtained and processed to develop the input to the numerical model.

The bathymetric data (30 arc-sec, 900 m resolution) was obtained from the database of British Oceanographic Data Centre GEBCO© (General Bathymetric Chart of the Oceans) and modified and improved by national navigational charts. Afterwards, the

dataset for land elevations were obtained with 30 m resolution using ASTER satellite website at https://gdex.cr.usgs.gov/gdex/. This topographical data is improved using the data collected from Bodrum Municipality.

In the simulations three nested grids are used. The largest domain used in the tsunami simulations was designated within the boundaries 27.25° - 27.55° E and 36.84° - 37.05° N with the spatial grid size of 15m (Figure 4.1).

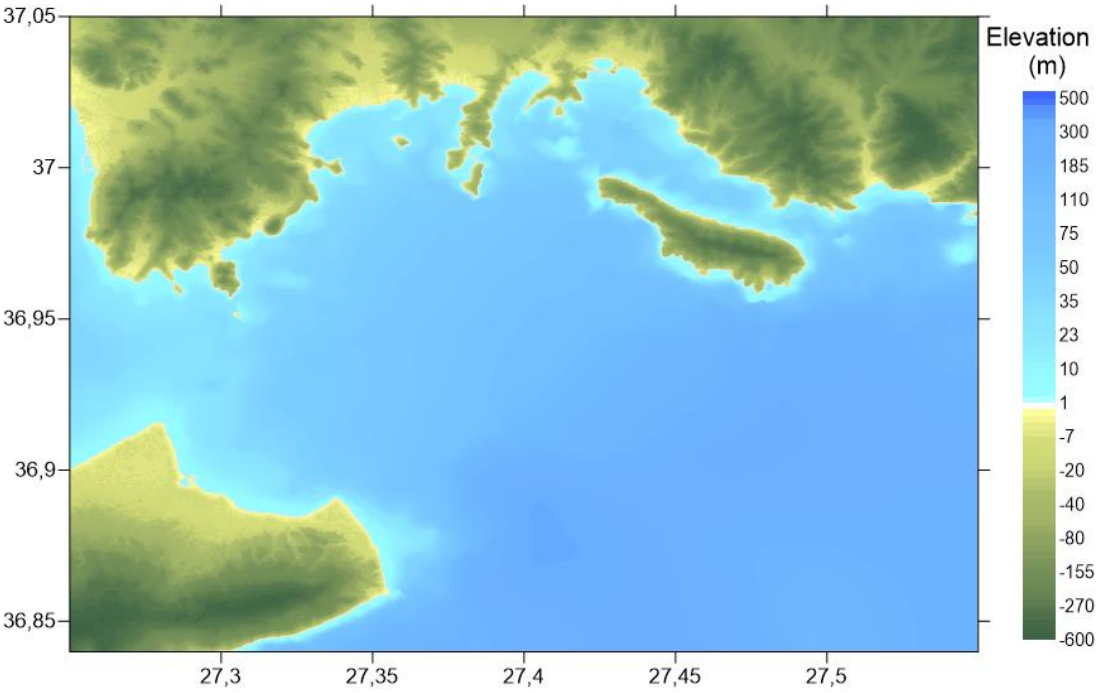

Figure 4.1. Map of the Bodrum-Kos tsunami domain used in the simulations

In order to have a consistent and precise computation between Bodrum-Kos tsunami domain and the Gumbet Bay, a smaller nested domain area is selected where the fragility functions for the damaged vessels are studied. Gumbet domain covers Gumbet Bay in the boundaries 27.38604° - 27.41260° E and 37.01415° - 37.03492° N with a grid size of 5m. The nested domain is shown in the Figure 4.2.

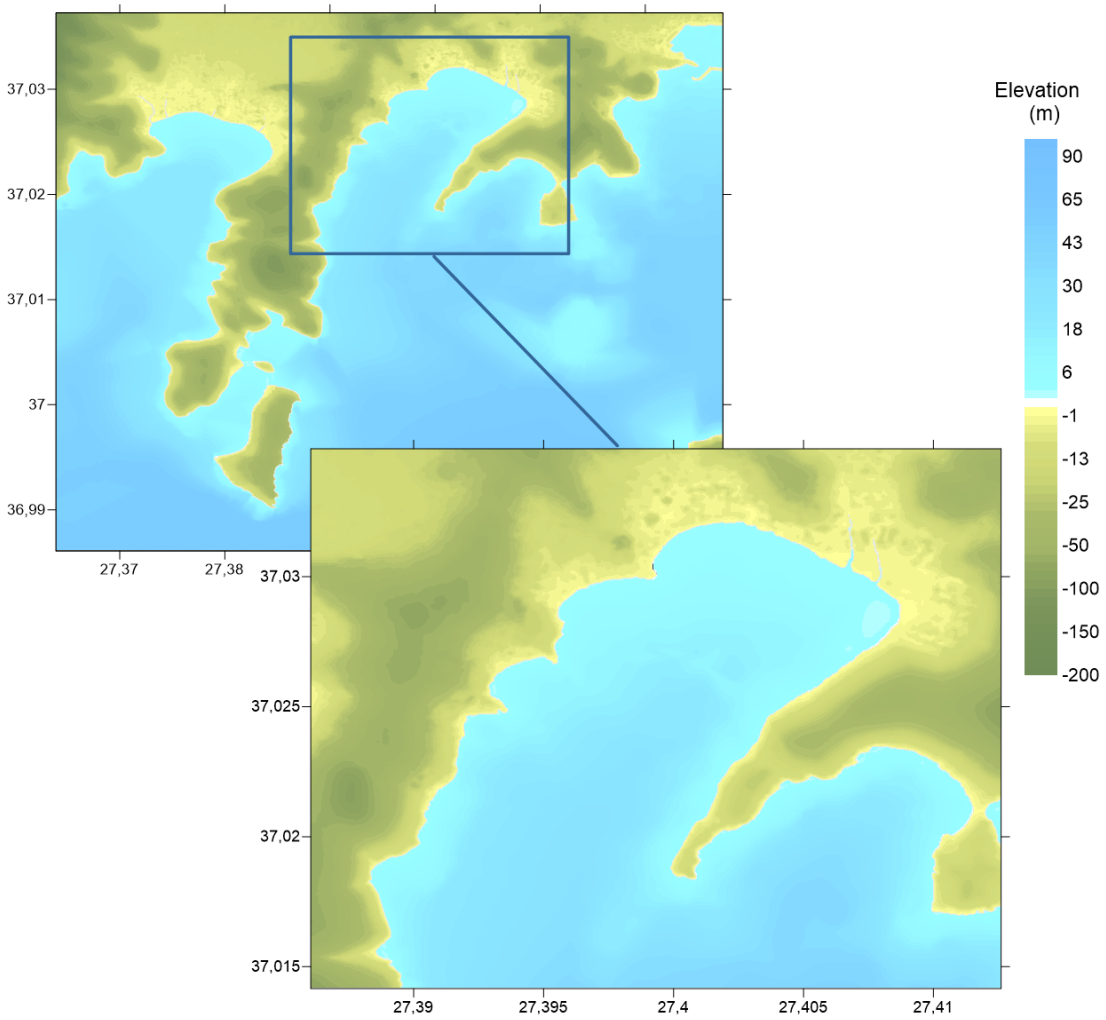

Figure 4.2. Map of the nested area (Gumbet domain) with 5m grid size

A wide number of gauge points are selected in Gumbet Bay in the computations to obtain tsunami parameters at various locations where the boats were damaged. During the selection of the gauge locations, the field survey locations given in Yalciner et al., (2017) and Dogan et al., (2019) are examined to select locations of the points where tsunami is observed by eyewitnesses or measured. In the Gumbet domain where the loss function is studied, gauge locations are selected at every berthing place where boats are moored. The locations of selected gauge points are presented in Figure 4.3. In addition, one point at the entrance of Bodrum Marina (GL1), where strong current

is reported by observers, and three points at the berthing places (bp1_3, bp8_2, bp16_3), in total 4 sample gauge points are chosen to show tsunami parameters after the simulations. The names of the gauges at these points are given in Figure 4.4.

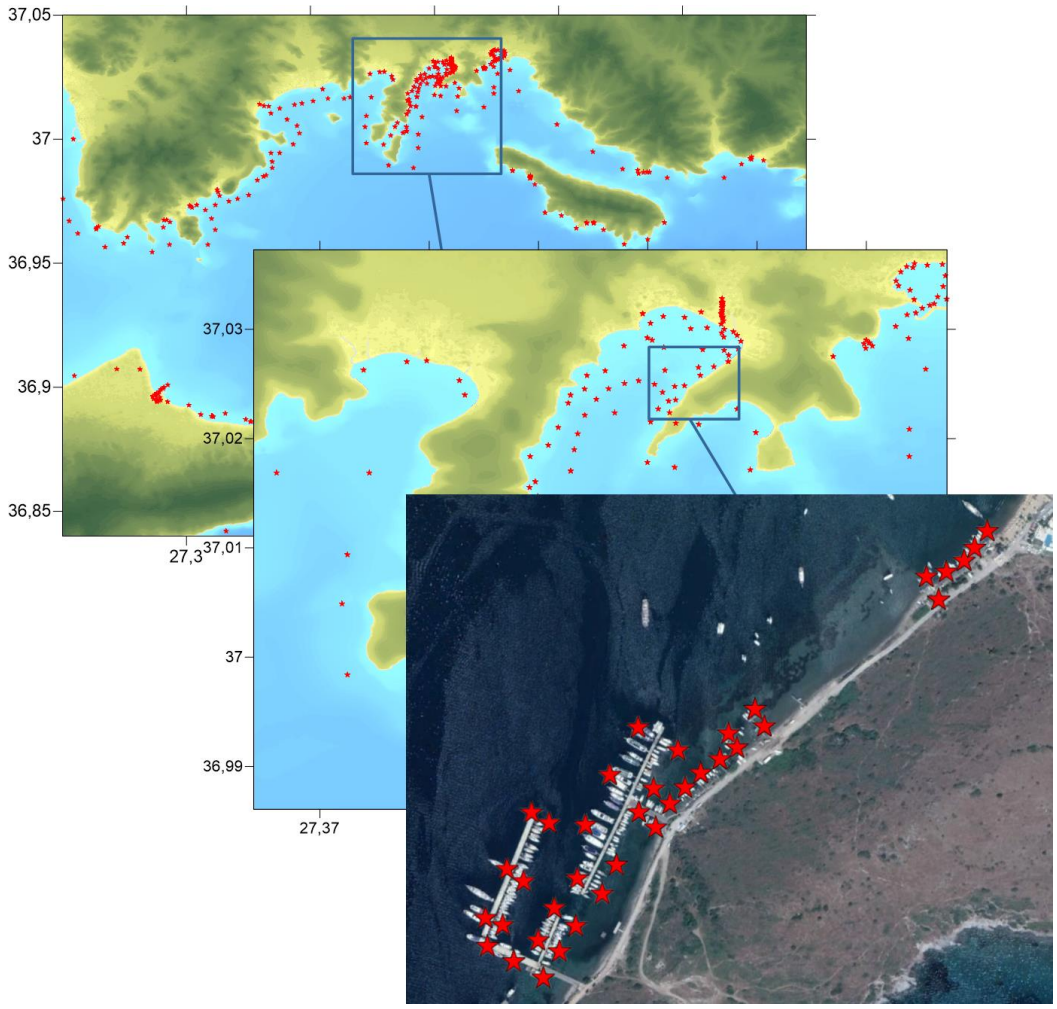

Figure 4.3. Position of the gauges used in the Bodrum-Kos and Gumbet Domain simulations

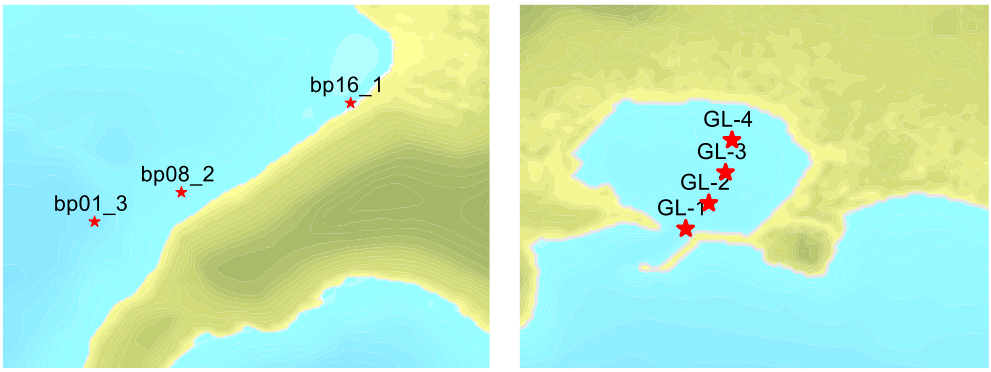

Figure 4.4. Name and location of the gauges given as sample points

4.1. Source Models

Fault parameters and possible source models of the tsunami is discussed by previous studies and the two approaches of dip polarity are determined as; south dipping (Saltogianni et al., 2017; Tiryakioğlu et al., 2018) and north dipping (Ganas et al., 2017; Karasözen et al., 2018). Another approach has been proposed by Prof. Dr. Ahmet Cevdet Yalciner as an elliptic subsidence with a maximum subsidence of 0.5m (Yalçıner et al., 2017). These three source models are explained in detail in the following sections.

4.1.1. Source Model with South Dipping Plane

Saltogianni et al. (2017) analyzed seismological and geodetic data simultaneously and obtained Finite Fault Models (FFM) of the Kos-Bodrum earthquake for computation of the variable slip model utilizing broad-band P- waveforms. Cause of the earthquake is identified as a 25 km long normal fault that ruptured from the sea bottom to 12 km depth along the upper crust. They resulted that the fault strike is approximately in E-ESE direction with a southerly dip.

Using the fault parameters defined by Saltogianni et al. (2017) a source model with south dipping plane is obtained (Fig. 4.5) and used for the simulations.

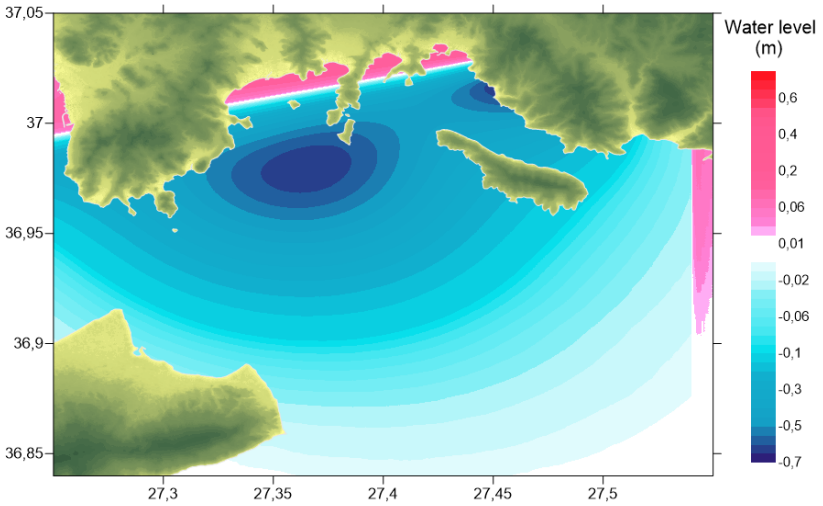

Figure 4.5. Source model with South dipping nodal plane in Bodrum-Kos domain

After 60 min simulation, the distribution of maximum water level in Bodrum-Kos domain is computed for South dipping source model and shown in Fig. 4.6.

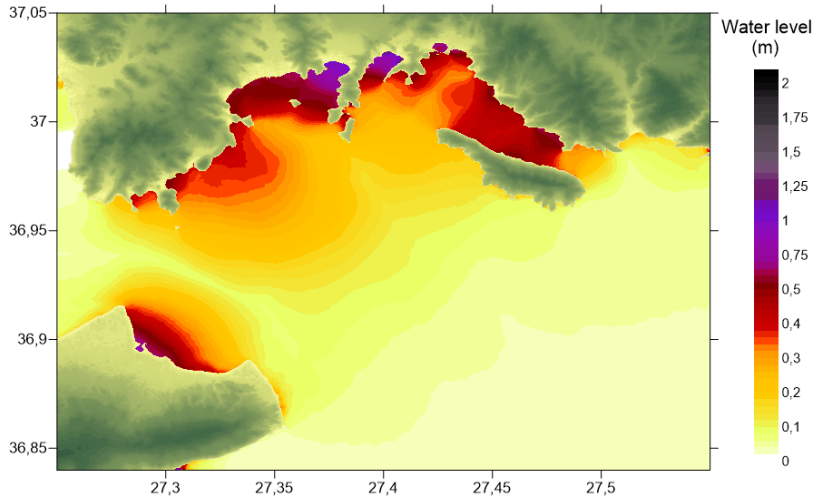

Figure 4.6. Distribution of maximum water levels in Bodrum-Kos domain computed in the simulation according to South dipping model

The results of the simulations with the south dipping plane model is also examined in regards to current and the water level changes in various gauge points. To illustrate better, time histories of water elevations (η) and current speeds are plotted (Fig. 4.7) at the entrance of Bodrum Marina (GL1) and 3 points in Gumbet Bay (bp01_1, bp08_2 and bp16_1). Bodrum Marine

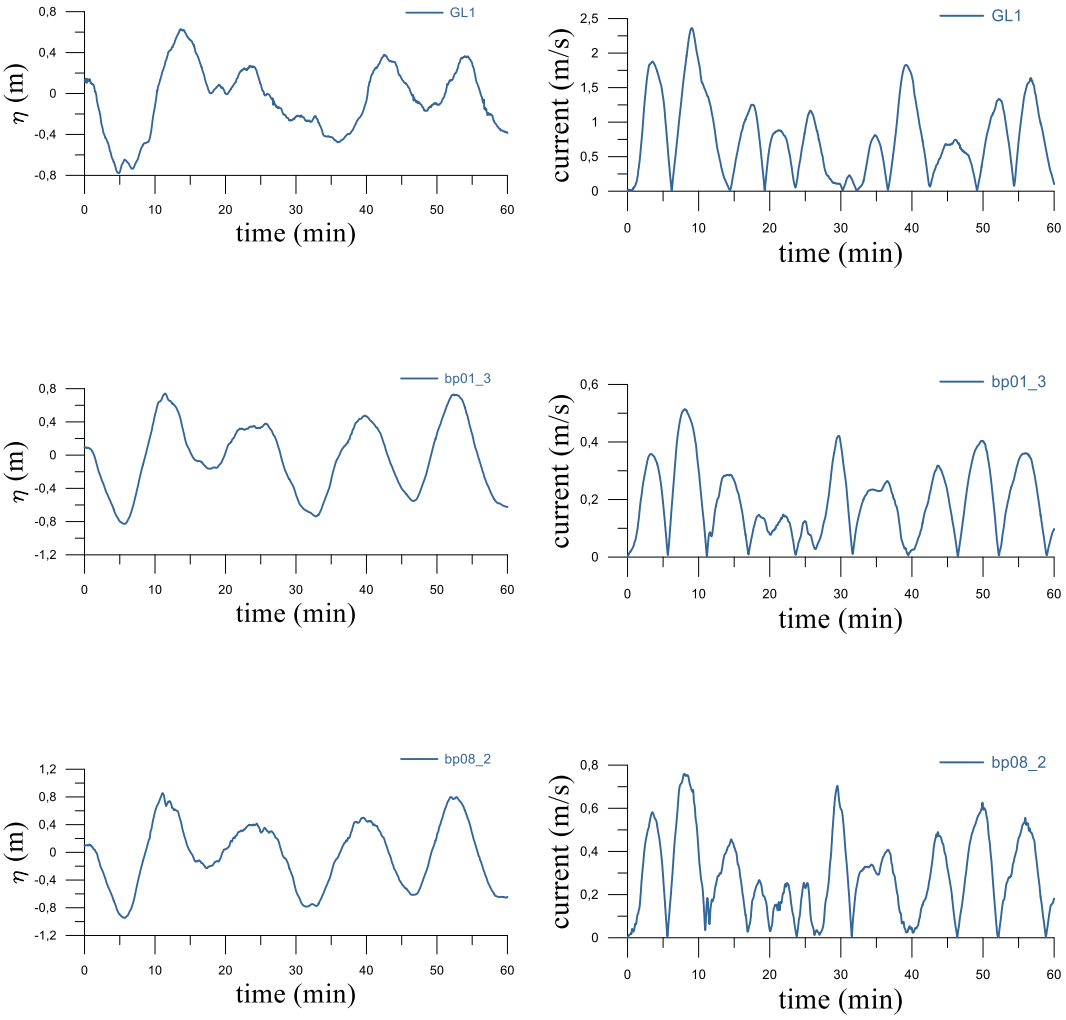

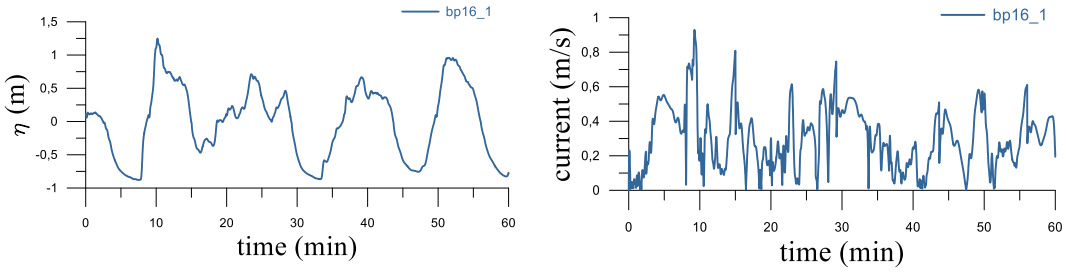

Figure 4.7. Time histories of water elevation (left) and current velocity (right) at sample gauges according to South dipping model

4.1.2. Source Model with North Dipping Plane

(Karasözen et al., 2018) states in their study that earthquakes with magnitudes up to Mw 6-7 can only be caused by the rupture of Gökova and North Datça faults. As a result, they propose that the faulting mechanism associated with the 2017 Bodrum-Kos earthquake was dominated by the N-dipping North Datça normal fault in the west rather than S-dipping Gökova normal fault in the eastern graben.

In addition, NOA suggests a source model with both north and south dipping nodal planes. The source model with north dipping plane used in the simulation is based on Finite Fault Models (FFM) suggested by NOA with 405 sub faults (27x15 of dimension) and 7 km focal depth. Figure 4.7 shows the north dipping plane source obtained from NOA's FFMs.

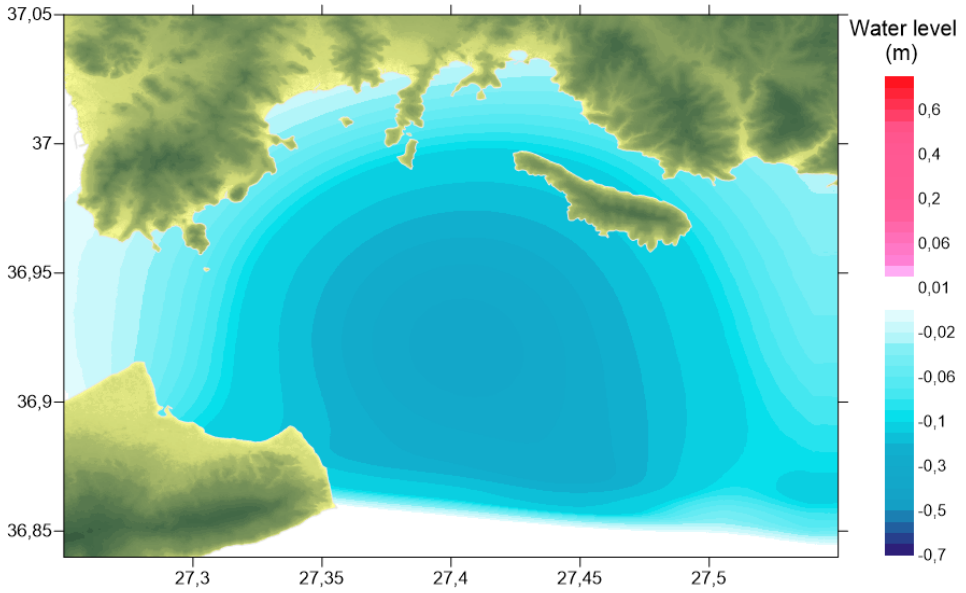

Figure 4.8. North dipping source model used in the simulations

After 60 min simulation, distribution of the maximum water levels among Bodrum-Kos domain is computed for North dipping plane source model (Fig. 4.9).

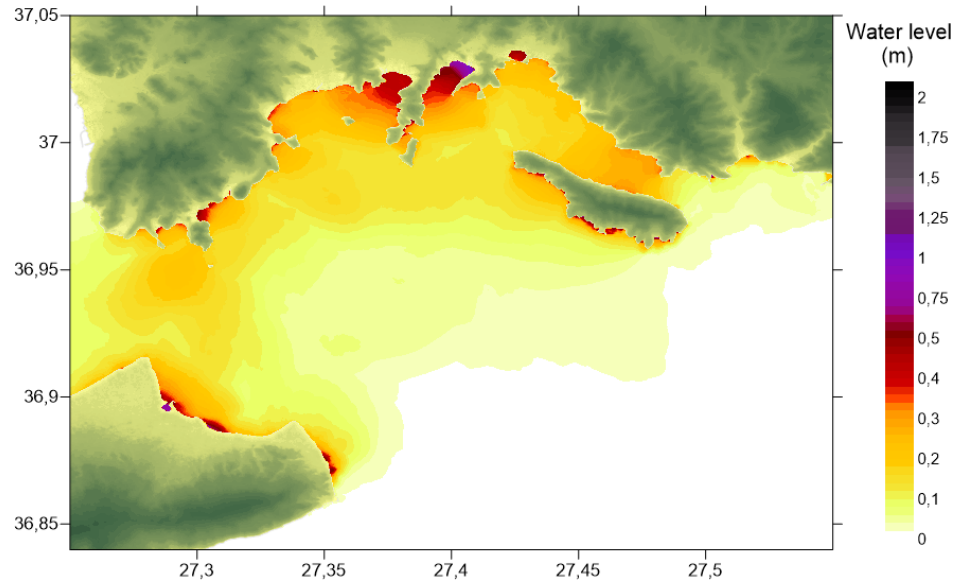

Figure 4.9. Distribution of maximum water elevations in Bodrum-Kos domain computed in the simulation according to North dipping plane source model

The results of the simulations with the source model based on North dipping nodal plane is also examined in regards to current speed and the water elevation of tsunami in various gauge points. To illustrate better, time histories of water elevations (η) and current speeds are given (Fig. 4.10) by the gauges same as the previous section with 3 points in Gumbet Bay (bp1_3, bp8_2, bp16_1) and a point at the entrance of the Bodrum Marine (GL1) where damaged boats are mostly located for comparison.

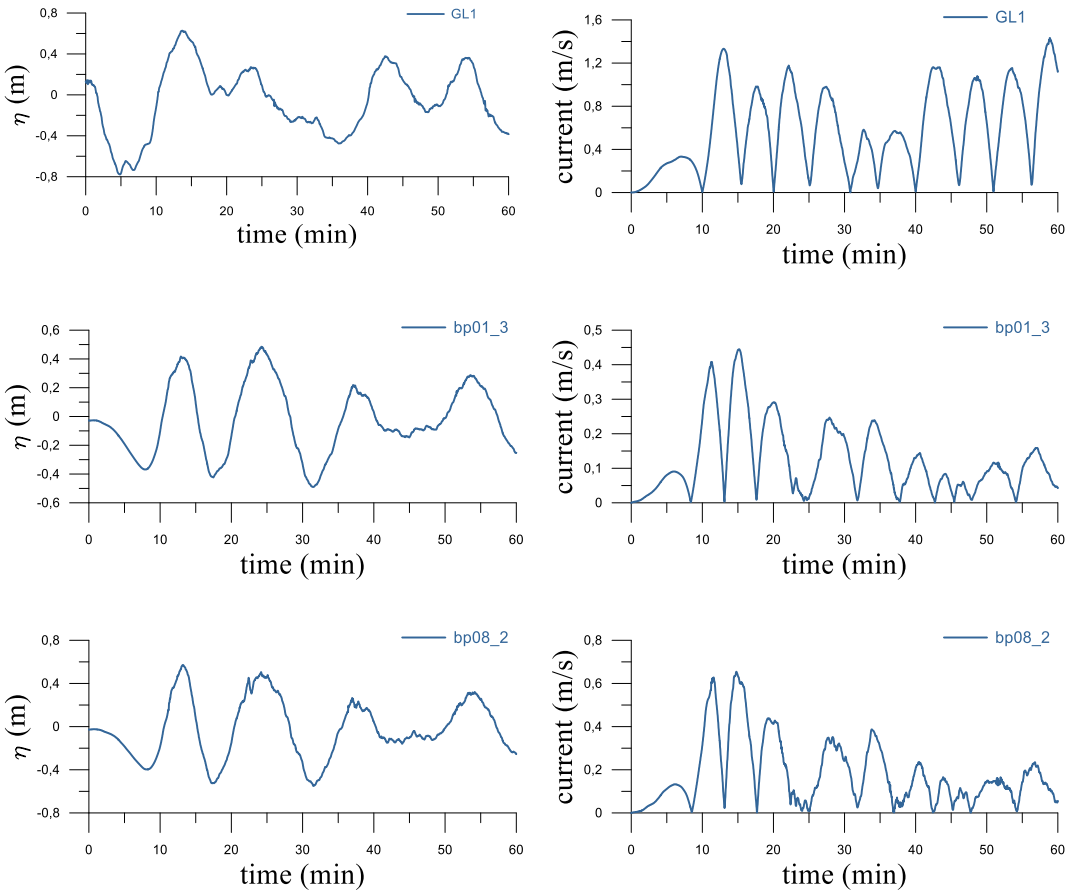

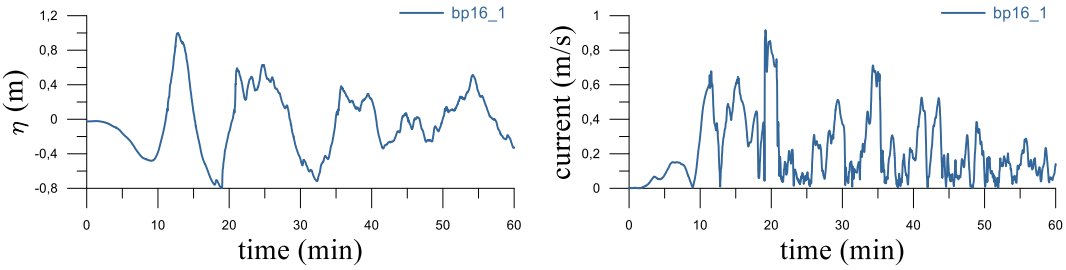

Figure 4.10. Time histories of water elevations (left) and current speeds (right) at sample gauges according to North dipping plane source model

4.1.3. Elliptic Source Model

Another source model with elliptical subsidence was proposed by Prof. Dr. Ahmet Cevdet Yalciner. The coordinate of the source center of semi ellipsoid subsidence is 27.423 East and 36.923 North. The major axis is along the direction 121-degree CW from North with a 12 km major axis length and 6 km of minor axis length. The subsidence is 0.5 m along the major axis, zero at the boundaries of the ellipse. The visual representation of the source is shown in Figure 4.11.

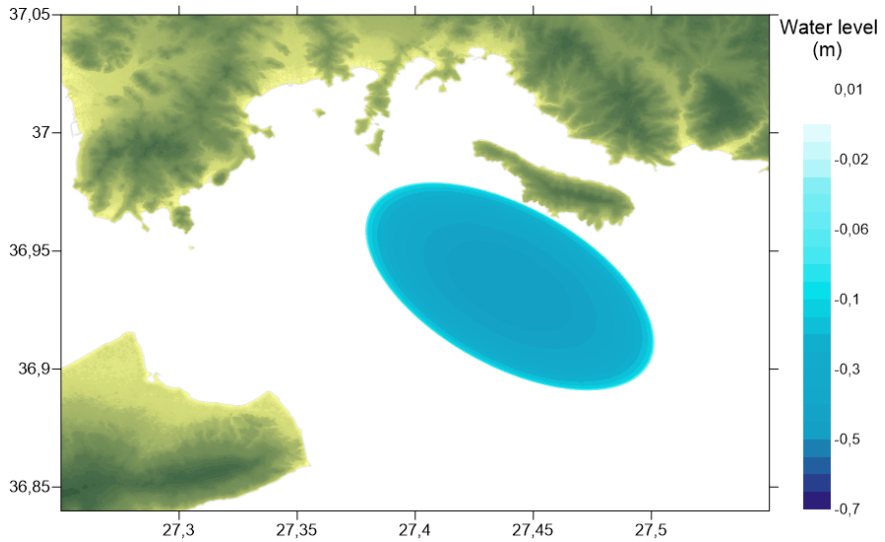

Figure 4.11. Elliptic source model used in the simulations

After 60 min simulation, distribution of the maximum water elevations in Bodrum-Kos domain is computed for elliptic source model and shown in Figure 4.12.

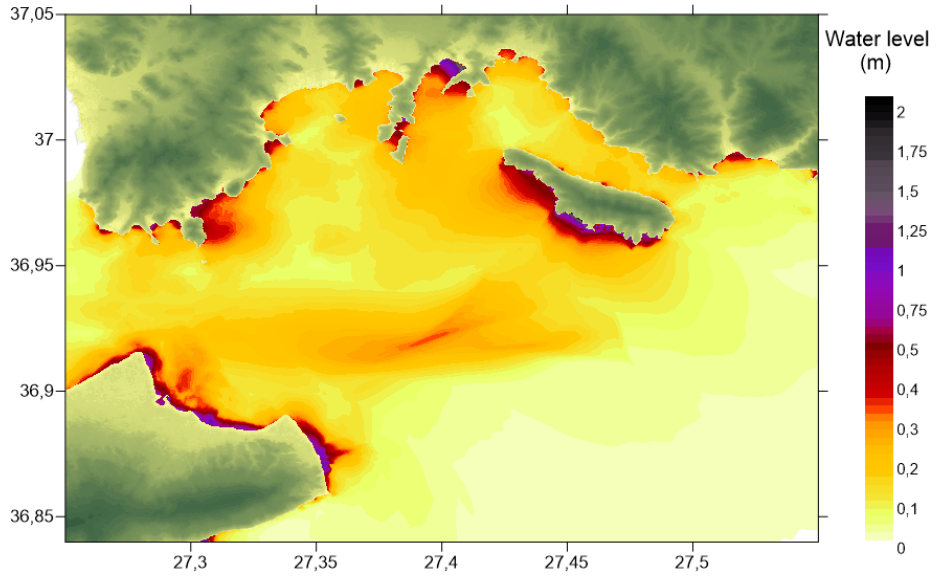

Figure 4.12. Distribution of maximum water elevations in Bodrum-Kos domain computed in the simulation according to elliptic source model

Likewise, the previous source models with the south and north dipping plane, the results of the simulations with elliptic source model is examined with respect to current velocity and the water elevation in numerous gauge points. In addition, time histories of water elevations (η) and current velocities are given (Fig. 4.13) by the gauges same as the previous source models with 3 points in Gumbet Bay (bp1_3, bp8_2, bp16_1) and a point at the entrance of the Bodrum Marine (GL1).

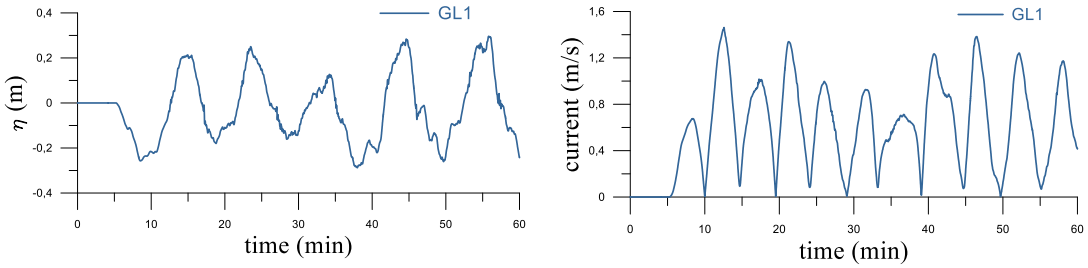

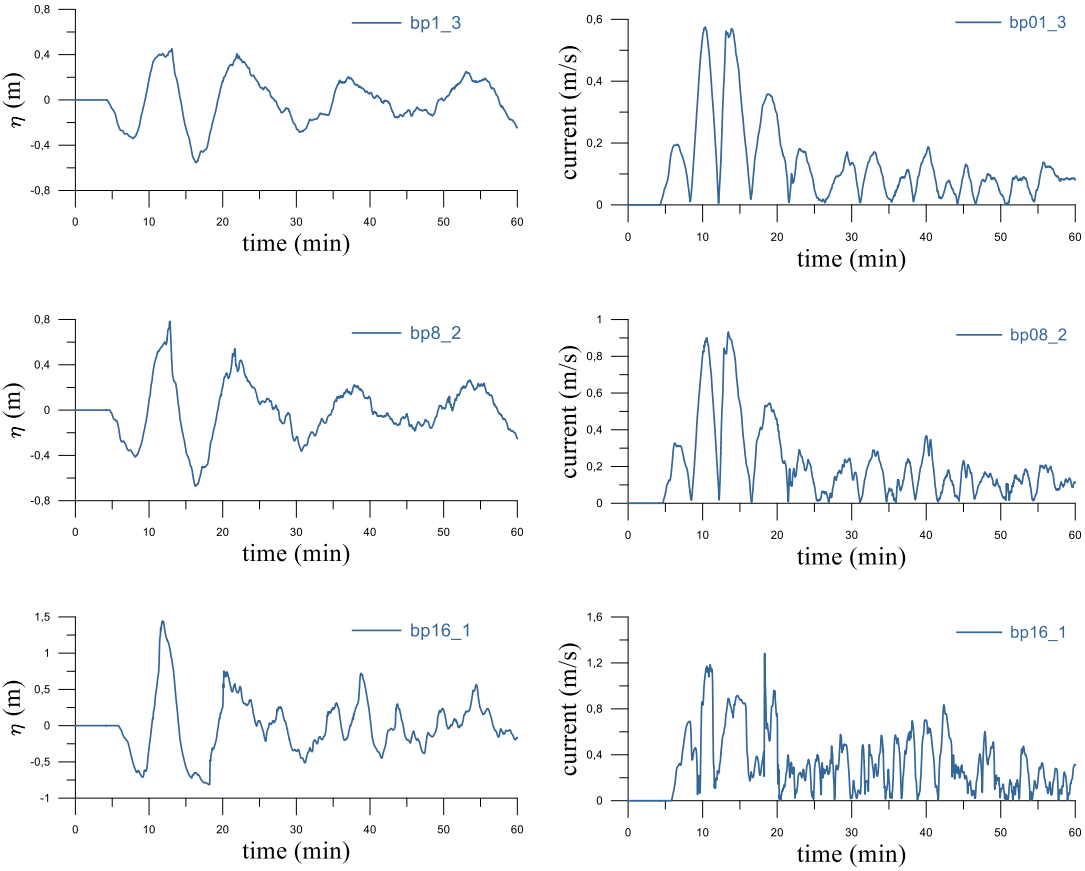

Figure 4.13. Time histories of water elevations (left) and current speeds (right) at sample gauges according to elliptic source model

4.2. Simulation Results

After computation of the tsunami parameters with 3 different source models performing 60-minute simulation by NAMI DANCE, the results for each source model have been compared with field survey observations.

In terms of water elevation, South dipping source model created the largest waves in Bitez Bay and Bodrum Marina. Moreover, it created the strong current velocities at the entrance of Bodrum Marina resulting in 2.5 m/s. However, along the east coast of Gumbet Bay, where the damaged boats are found, current velocities remained under 1m/s while water elevations were mainly below 0.7 m. Furthermore, arrival times of

the initial and maximum waves to the berthing places at Gumbet Bay computed to be around 3 to 4 minutes and 10 minutes respectively, which are less than the observed arrival times (5 min and 13 min). Therefore, the results are not compatible with the observed parameters and are not able to satisfy the criteria for boat damages.

North dipping source, on the other hand, resulted in relatively smaller current velocities and water elevations compared with the South dipping model. Especially at the entrance of Bodrum Marina, North dipping source model created currents up to 1.5 m/s. Even though it is much smaller than the current with 2.5 m/s computed by south dipping model, it still holds the capacity to drag boats. It can be concluded that this source model produced quantitatively satisfactory waves, nevertheless, the outcomes of water level and current velocity along the berthing places failed to satisfy the capacity that may cause the reported damages.

Elliptic source model, similar to the North dipping source, produced a current with 1.5 m/s in Bodrum Marina. In contrast, water elevation computed in Gumbet Bay found to be up to 1.5 m which is more compatible with the statements of eyewitnesses than other two source models. Additionally, when compared to the other models, elliptic source created stronger currents (up to 1.5 m/s) along the berthing places in Gumbet Bay region where damaged boats were located. Moreover, arrival times of the first and maximum waves are found to be 5 min and 13 min respectively as reported in the field survey report. In other terms, elliptic source generated satisfactory tsunami parameters which are consistent with the field survey and capable of causing boat damage. Thus, the parameters generated by the elliptic source is decided to be used in the following calculations and vulnerability analysis within this study.

The distribution of maximum and minimum water elevations in Gumbet domain are shown in Figure 4.14 and Figure 4.15. Distribution of maximum current velocity is shown in Figure 4.16 as well as the distribution of maximum flow depth in Gumbet domain is given in Figure 4.17.

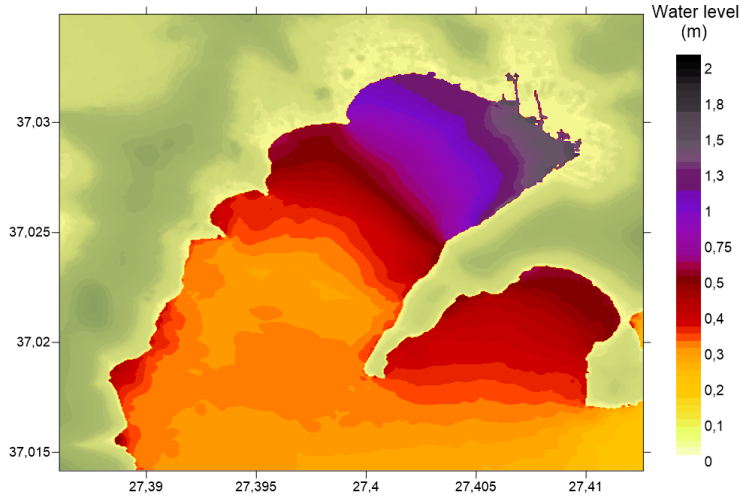

Figure 4.14. Distribution of maximum water levels in Gumbet domain computed by the simulation due to elliptic source model

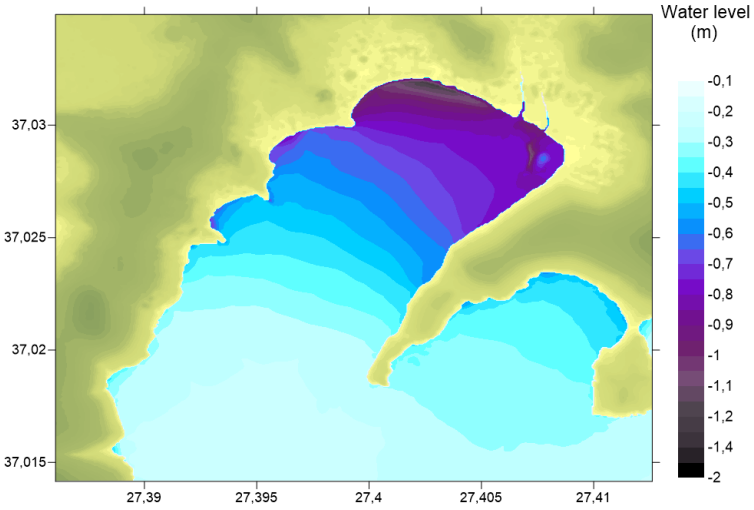

Figure 4.15. Distribution of minimum water levels in Gumbet domain computed by the simulation due to elliptic source model

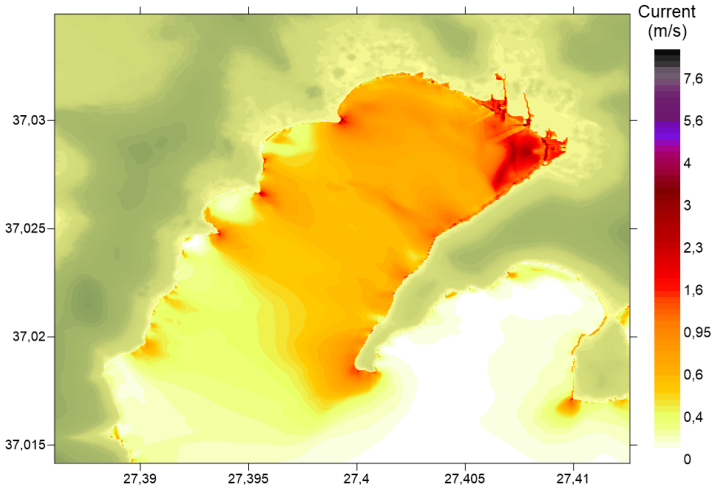

Figure 4.16. Distribution of the maximum current velocities in Gumbet domain computed by the simulation due to elliptic source model

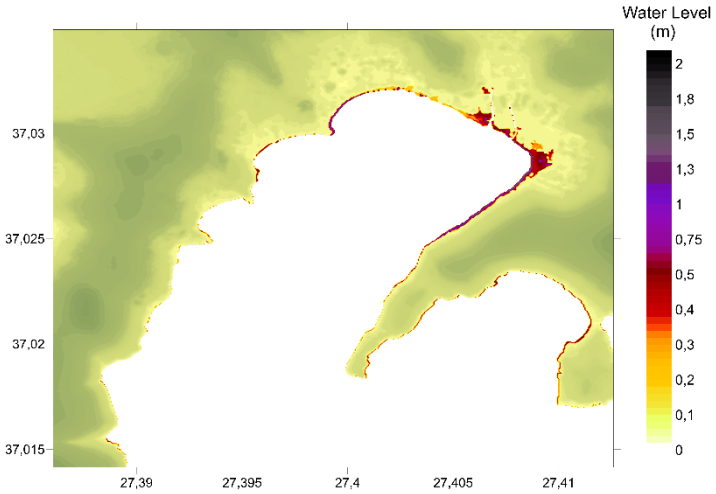

Figure 4.17. Distribution of the maximum flow depth in Gumbet domain computed by the simulation due to elliptic source model

To demonstrate further, a representative gauge point at every berthing place is selected and time histories of water elevations and current velocities at these points are plotted. Figure 4.18 shows the locations and the names of the gauge points and Figure 4.19 presents the time histories of water elevations and current velocities. As it can be seen from the figures that water elevations and current velocities are increasing towards the

eastern end of the Gumbet Bay. The values of the water elevation and the current velocity reaches up to 1.5 m and 1.4 m/s respectively along the berthing places bp14, bp15 and bp16. These points are also the points that the most vessel damages are observed according to tsunami field survey.

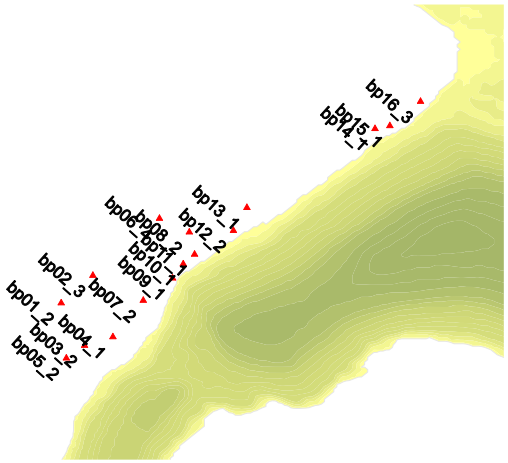

Figure 4.18. Representative gauge points at every berthing place in Gumbet Bay

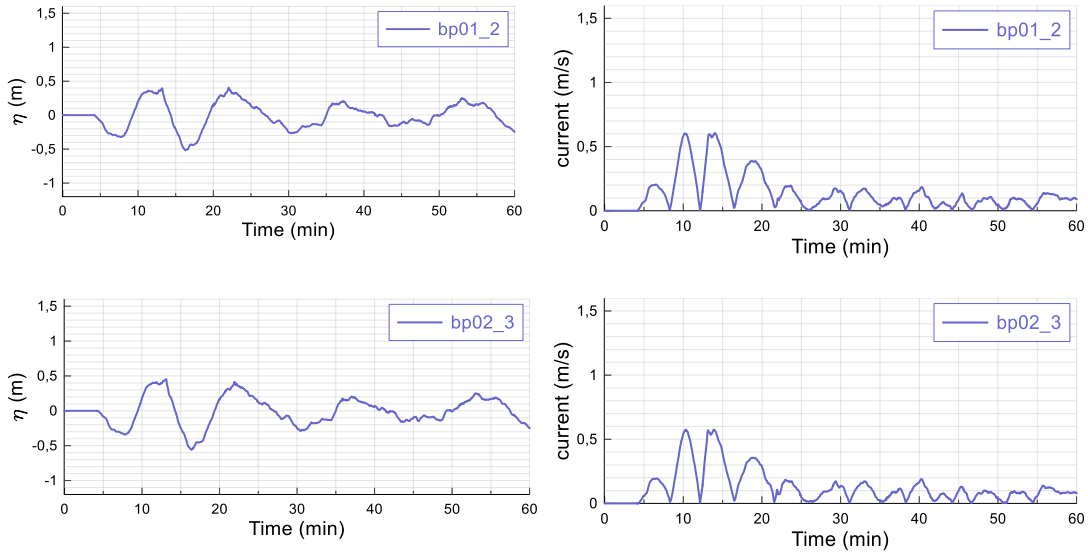

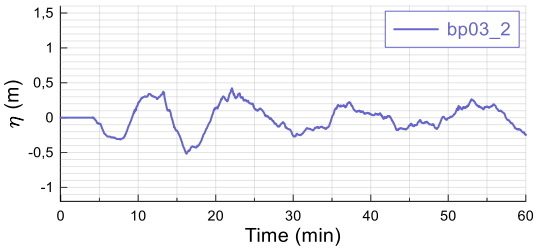
bp03_2
η (m)
Time (min)

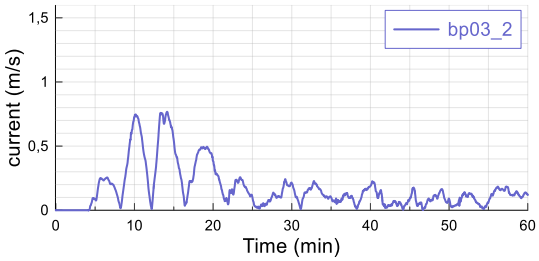
bp03_2
current (m/s)
Time (min)

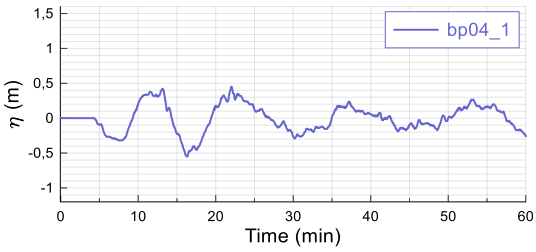
bp04_1
η (m)
Time (min)

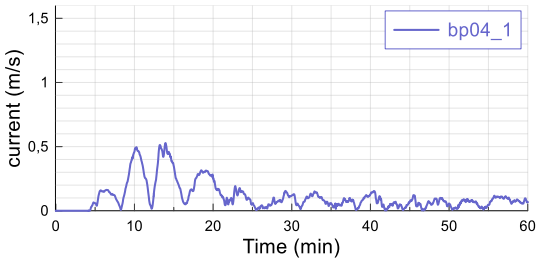
bp04_1
current (m/s)
Time (min)

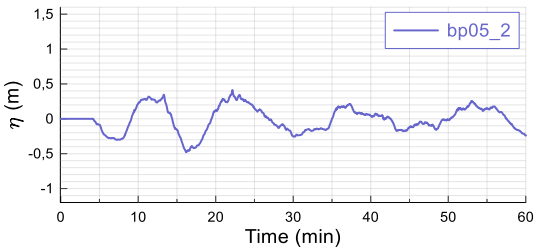
bp05_2
η (m)
Time (min)

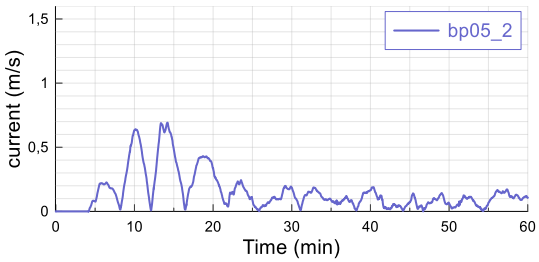
bp05_2
current (m/s)
Time (min)

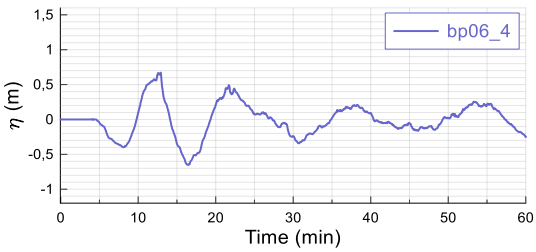
bp06_4
η (m)
Time (min)

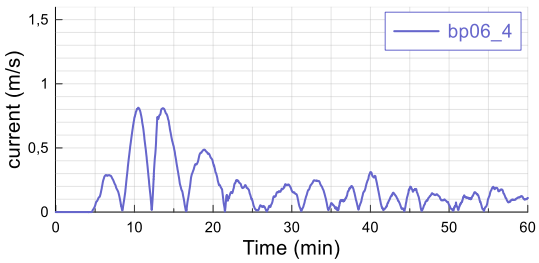
bp06_4
current (m/s)
Time (min)

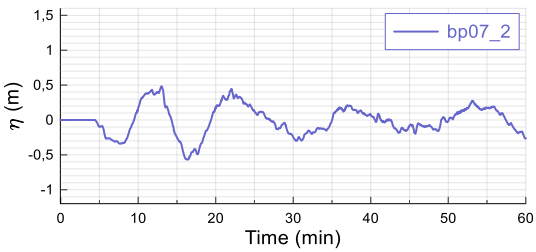
bp07_2
η (m)
Time (min)

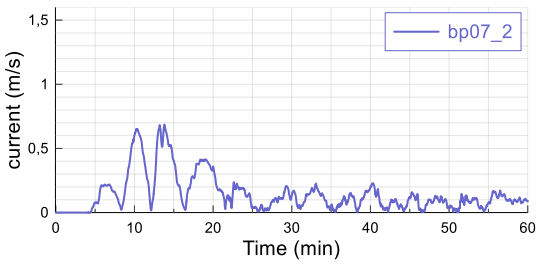
bp07_2
current (m/s)
Time (min)

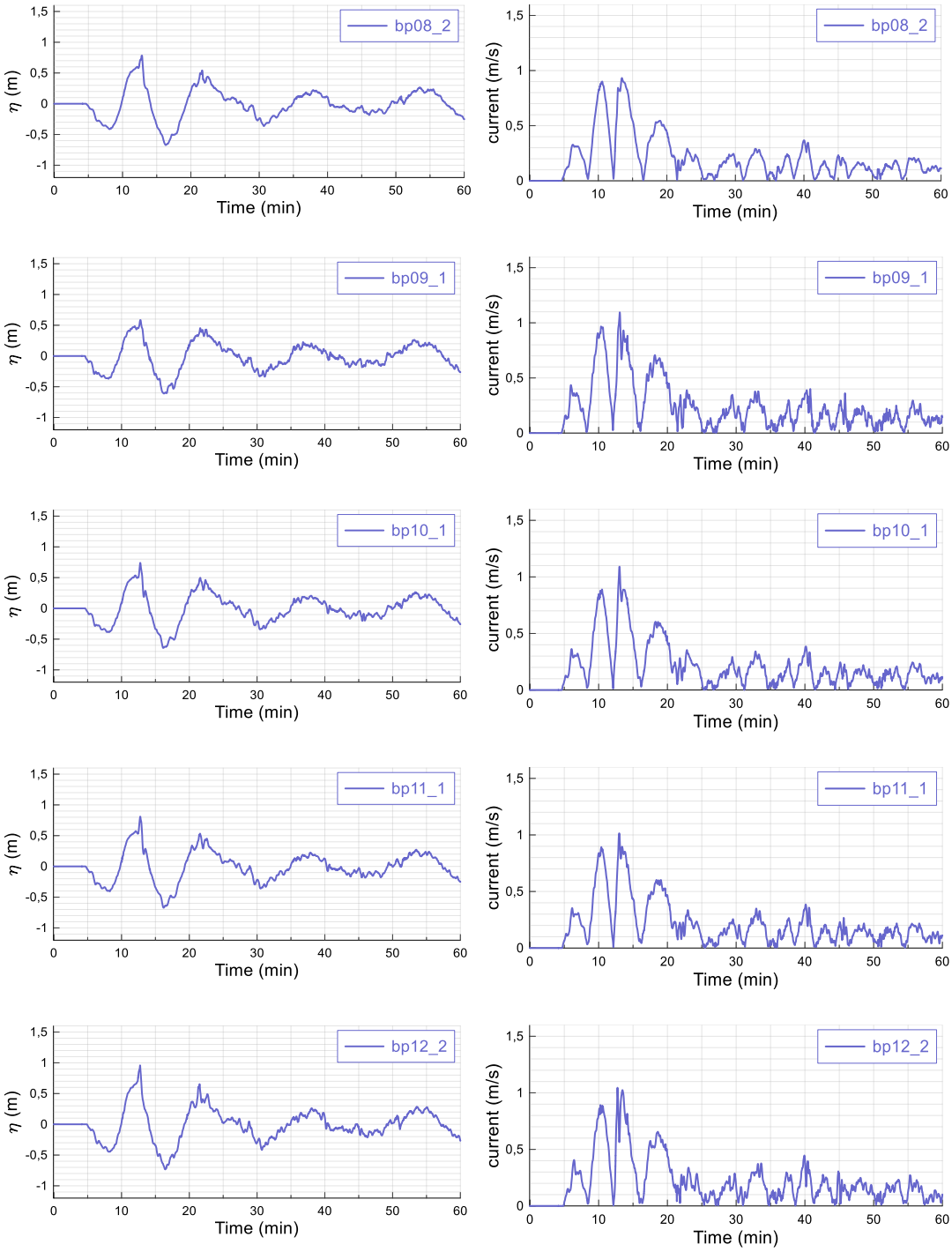
bp08_2
η (m)
current (m/s)
Time (min)
bp09_1
bp10_1
bp11_1
bp12_2

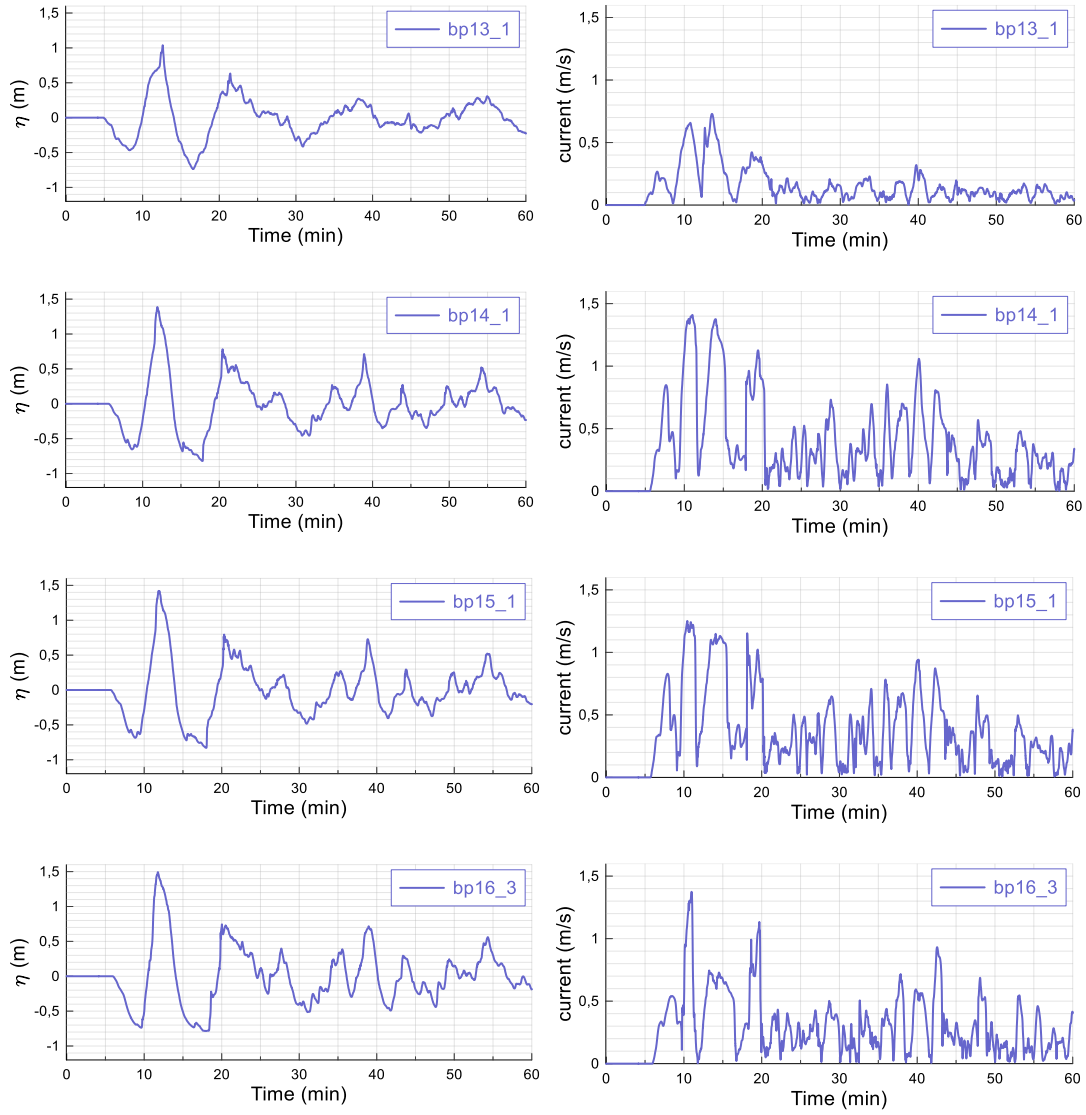

Figure 4.19. Time histories of water elevation (η) and current velocities due to elliptic source model at sample points from every berthing place

CHAPTER 5

VULNERABILITY ANALYSIS

Tsunami fragility and vulnerability functions are statistical models that provide us to predict an expected damage or losses due to tsunami. They allow us to estimate risk, and in a larger scope, they are significant elements of risk mitigation models and emergency planning used for decreasing human and financial loss (Charvet, Macabuag, & Rossetto, 2017).

The components of tsunami risk can be listed as tsunami hazard, vulnerability and exposure. If we adopt the risk definition used by Crichton, (1999) and apply them for the tsunami hazard on marine vessels, the components for the tsunami risk can be explained as below;

Tsunami hazard = the probability of potentially damaging tsunami occurring at a place within a given period.

Vulnerability = The likelihood of losses to marine vessels for a tsunami with particular intensity.

Exposure = Quantification of the number of vessels at risk.

In addition, vulnerability of vessels depends on two elements; fragility and loss model. Again, applying definitions for vessel vulnerability, fragility can be expressed as the probability of vessel damage for a certain tsunami intensity. In our case, loss model cannot express a certain financial loss but it may give us a probable relationship with predefined level of vessel damage.

Tsunami parameters to be used as tsunami intensity measures in the fragility analysis have been obtained and given in Chapter 4 however, to carry out a decisive analysis on the boat damages, it is needed to consider many factors that can have an effect on

the fragility of the vessels. In order to achieve an explanatory statistical model, multiple variables including vessel properties required to be employed in the analyses both individually and simultaneously. Therefore, gathering information about the vessel properties was essential to obtain relevant variables to develop this multivariate statistical model.

Furthermore, to explain vessel damage in a more analytical way, a fundamental classification of the damages or damage ratios has been necessary. As a result, a detailed analysis of the damaged vessels and respective damage classifications at the berthing places at Gumbet Bay has been performed and given in this chapter.

5.1. Estimation of Vessel Properties

The number of vessels with their sizes, materials and tonnage are determined and given in this section. First of all, satellite images taken from Google Earth in various dates before and after tsunami and the statements of eyewitnesses are used to determine the number of vessels at each berthing place when the tsunami hit the region. Knowing that the earthquake occurred at 01:31 local time on a peak season day, it is confirmed that almost all of the boats were moored at the berthing places. For simplification berthing places are named from 1 to 16 (bp1, bp2 etc.) and Figure 5.1 shows the satellite images and location of the berthing places in Gumbet bay. All images deriven from Google Earth used in determination of measurements and numbers of vessels are given in Appendix.

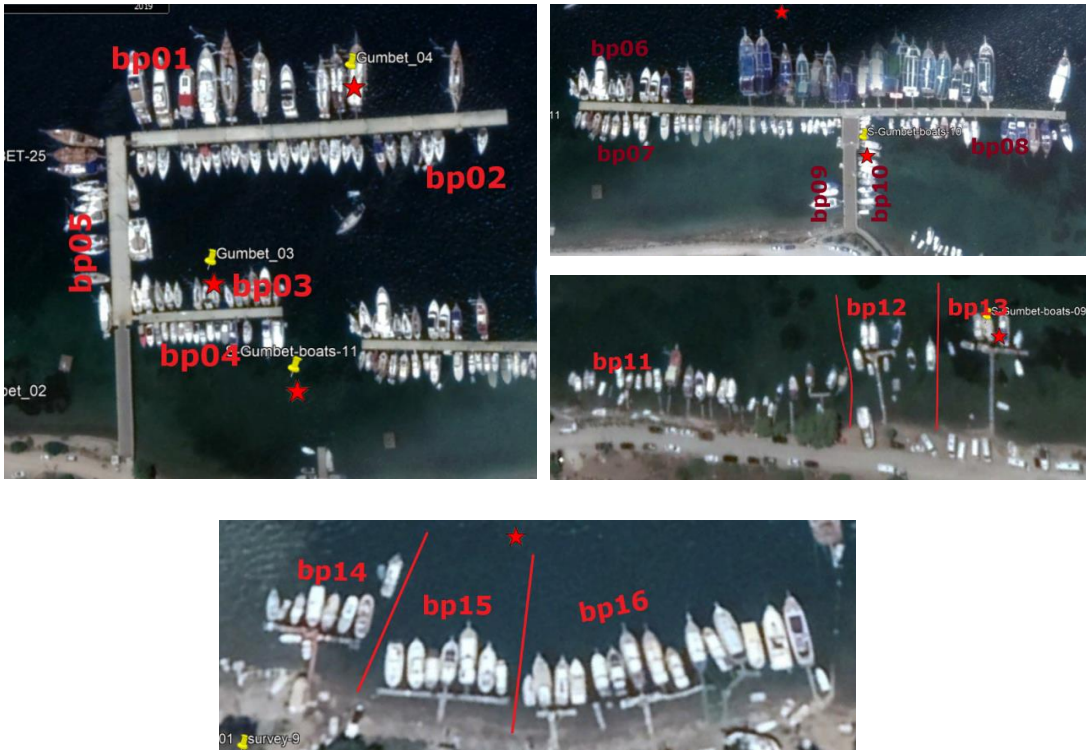

Figure 5.1. Satellite images of the boats at berthing places taken from Google Earth on June 20, 2017

After analyzing images taken on various dates from Google Earth images and conforming the number of vessels with their length and materials are obtained. As a result, total number of vessels included in the vulnerability study is determined as 305 with 47% of them is classified as fiber and %53 of them is classified as wooden.

5.2. Estimation of Tonnage

Weight of the boats is considered as a function of production material and the size of the vessel. Therefore, the relationship between the length and the weight of the vessels examined for the corresponding material (Yılmaz & Erol, 2015) and a second degree polynomial curve is fitted to the data as given in the plot in Figure 5.2. Using the formula of the fitted curve, corresponding tonnage for each vessel is calculated. Finally, the number of small vessels weighting less than 5 tons is found as 75% of all

marine vessels whereas the ones between 5 tons and 20 tons and large vessels weighting more than 20 tons are 15% and 10% respectively.

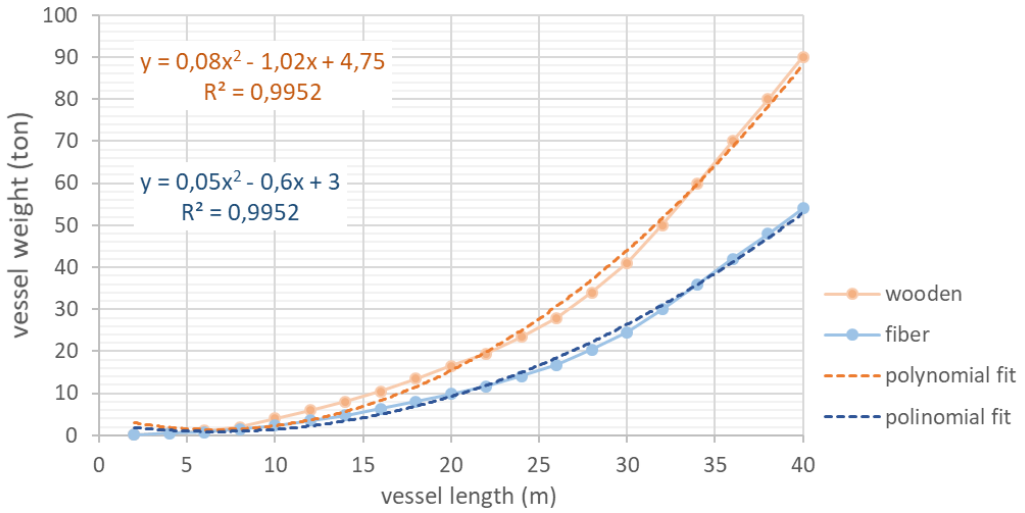

Figure 5.2. Relationship between vessel length and tonnage (adapted from Yılmaz & Erol, 2015)

5.3. Damage Classification

In addition to detailed examination of images taken during field survey, the marine workers have been interviewed to obtain the information on the number of vessels damaged. The different damage types caused by tsunamis have been defined such as grounding, stranding, failure of the mooring rope and loss of stability (Suppasri et al., 2014). Since receding of the water level at the berthing places was not sufficient, grounding could not have observed and not included in this case. Stranding is observed for some of the vessels where the tsunami height and the complementary buoyancy on the vessel is relatively greater so that the vessel moves above the pier level. Although simulated current velocities are smaller than 2 m/s, failure of mooring rope was observed in many boats. This can be mainly because of the mooring ropes were weak and most of the vessels were smaller than 5 tons. The most common damage type

among the small vessels (< 5t) was the loss of stability as all the boats were stationary at the moment of tsunami.

Figure 5.3 shows some of the images taken during survey after the tsunami at Gumbet Bay. Various damage types are observed and damage classifications are determined using more than 100 images and experience of the eyewitnesses.

Figure 5.3. Washed away, overturned and sunk boats at Gumbet Bay (Images taken by Gökhan Güler)

After determining damage types, the levels of damage of the vessels have been classified for explanation of the fragility. In general, the fragility function concept, which is used for structures provides a different type of classification since it considers damage of the structures. On the other hand, studies on the loss functions of marine

vessels define a damage ratio for marine vessels by means of their economic loss. In fact, the damage ratio is determined by the scale of paid insurance to the total insurance worth of a vessel (Muhari et al., 2015; Suppasri et al., 2014). However, the determination of a ratio based economic loss of the vessels in Gumbet Bay was not possible. Therefore, instead of using damage ratios, the fragility curves in this study were illustrated based on damage levels defined by Aketa et al. (1994, as cited in Suppasri et al., 2014).

Vessels are initially grouped as survived, damaged, and washed away. Later, damaged vessels are divided into three according to the state of damage as minor, moderate and major. Thus, 5 different damage levels assigned for each state in a scale from Level 0 to Level 4 are given in Table 5.1.

Table 5.1. *The scale of damage levels*

State of damage	*Damage level*
No damage	Level 0
Minor damage	Level 1
Moderate damage	Level 2
Major damage	Level 3
Washed away	Level 4

No damage classification is used for vessels that are not deteriorated by tsunami forces and represented as Level 0. Minor damage term represented as Level 1 defines the vessels that have exterior damage but require no repairment to function properly. Moderate damage term represents the vessels that require maintenance without transporting the vessel to any shipyard in the land. This damage level is assigned as Level 2. Major damage is used for the vessels that require extensive maintenance to function again thus it is required to be transported to land and shown by Level 3.

On the other hand, washed away term is independent from the damage levels that are mentioned above. Originally washed away term is created for the structural damage

and used to represent 100% loss of the structures in the structural fragility studies. However, the concept of the fragility of the marine vessels differs from the structural fragility in many ways. Therefore, washed away vessels do not necessarily contribute to 100% loss. In this study washed away classification is used for the vessels that separated from their mooring by tsunami force, dragged and found at another place. There were no missing vessels after the tsunami; thus there were no %100 loss in this event. Moreover, it is expected that the vessels are washed away under respectively higher values of tsunami forces. Because of these reasons, washed away vessels are considered to be the most vulnerable and so it is shown by Level 4.

After completing the damage examination of 305 vessels, the number of vessels at each damage level is determined. 71% of the vessels had no damage while minor, moderate and major damages contribute 12%, 8% and 5% respectively. 4% of all vessels washed away. The pie chart of the distribution of damage level of the boats in Gumbet Bay is shown in Fig. 5.4.

Damage level	*Number vessels*
Level 0	244
Level 1	25
Level 2	16
Level 3	10
Level 4	9

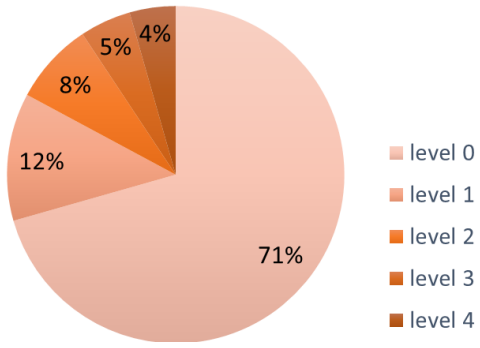

Figure 5.4. Distribution of damage levels

5.3.1. Damage Based on Vessel Properties

In order to analyze the effect of vessel properties on the damage, the data has also been categorized according to the type of vessel material (wood or fiber) and vessel size based on tonnage (smaller than 5 tons, between 5 and 20 tons and larger than 20 tons).

In this categorization, only damaged and washed away boats are included. 75% of all damaged or washed away vessels were found to be fiber and 98% of them were smaller than 5 tons (Fig 5.5).

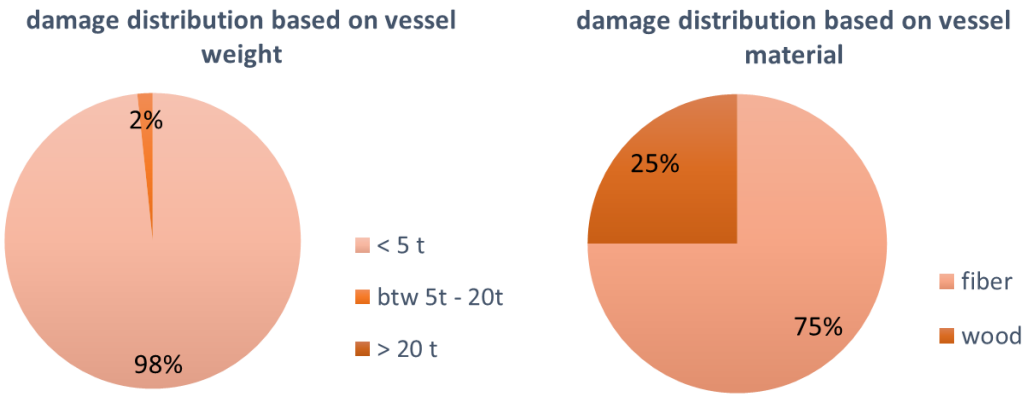

Figure 5.5. Distribution of the number of damaged or washed away vessels according to vessel properties

Since vessel material and vessel weight are the two key vessel properties, damage levels are categorized for different materials and different range of tonnage (Fig 5.6). The percentage of survived boats made of wooden materials are found considerably higher. In addition, almost all of the damaged vessels were smaller than 5 tons, whereas there were no damaged or washed away vessels bigger than 20 tons.

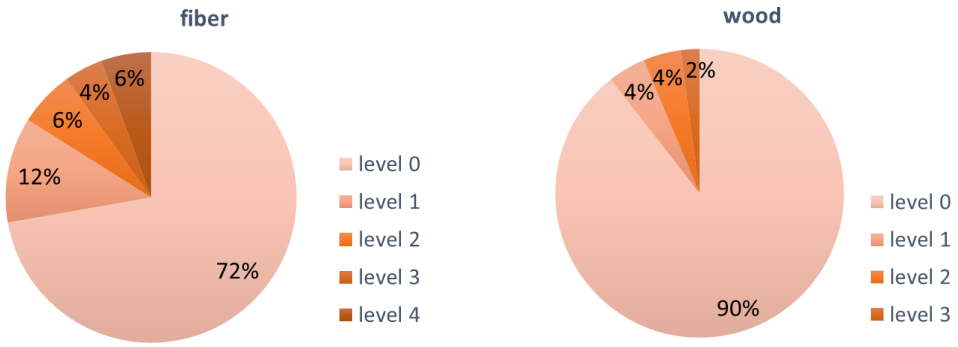

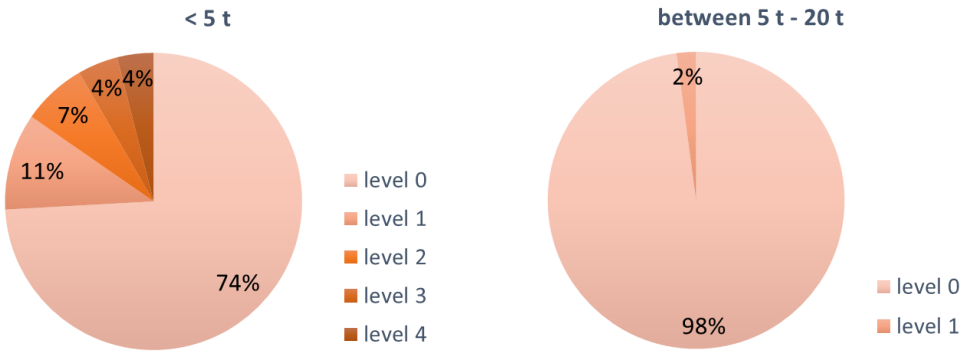

Figure 5.6. Damage levels according to material and tonnage

5.3.2. Damage based on Tsunami Parameters

Maximum water elevation and current velocity are the two different tsunami parameters, which are often used in the fragility functions. Figure 5.7 shows the distribution of all damage level data for these two contributing tsunami parameters.

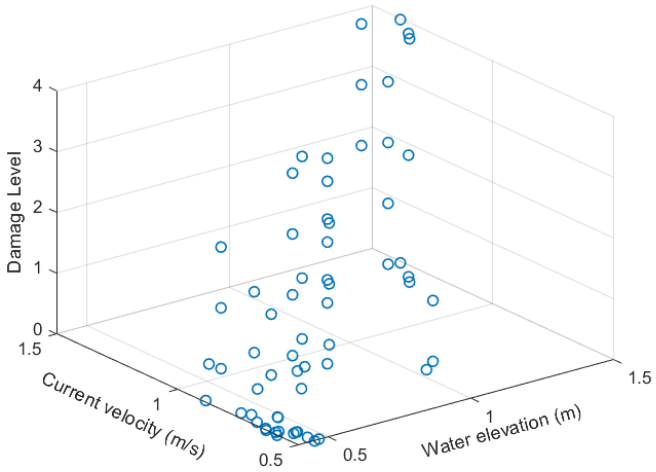

Figure 5.7. Distribution of damage levels according to water elevation and current velocity

In order to have a better understanding in fragility curves, initially a statistical analysis is needed. Therefore, for each damage level, the histograms of maximum water elevation and current velocity are obtained and the damage level data is re-arranged with respect to contributing current velocity and water elevation. Figure 5.8 and 5.9 show the histograms for each damage level based on maximum water elevations and maximum current velocities respectively. It can be concluded from these plots that vessels are only washed away when the tsunami height (water elevation) and current velocity are greater than 1.3 m and 1.2 m/s respectively. In addition, major damage is only observed when the tsunami height (water elevation) and current velocity are greater than 0.7 m and 0.9 m/s respectively. On the other hand, no clear relation could be observed for damage level 1 and 2 by the representing histograms. Thus, fragility curves are needed to understand the relation between tsunami parameters and damage levels.

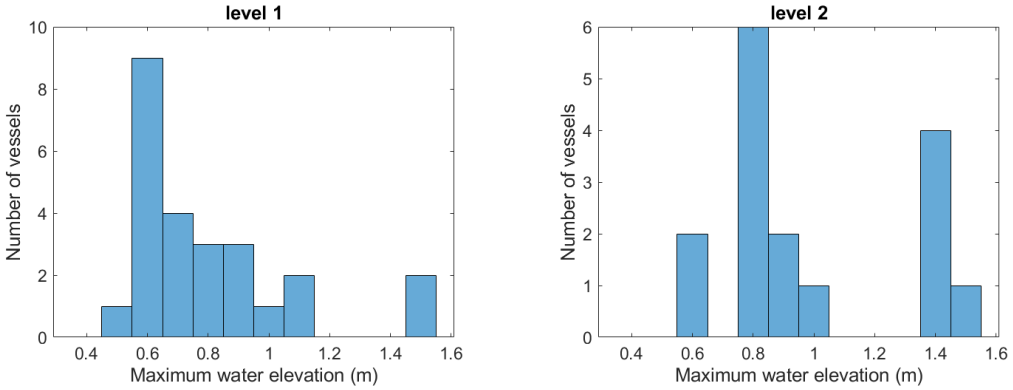

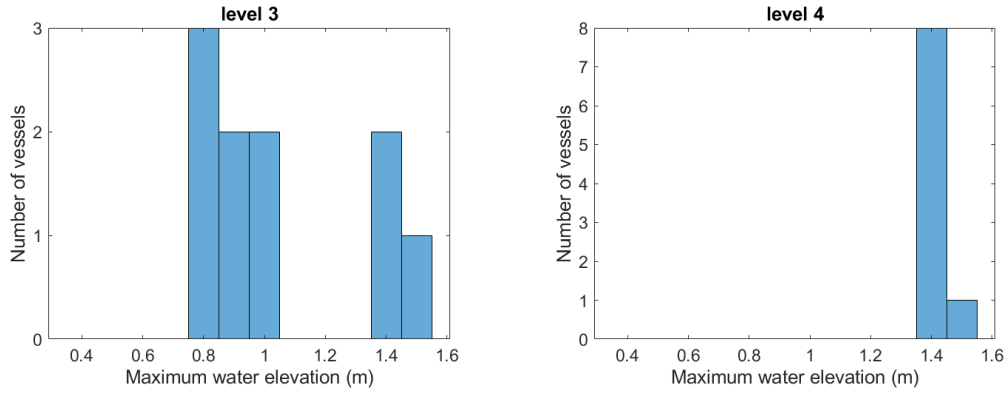

Figure 5.8. Number of damaged vessels for different maximum water elevation ranges based on damage level

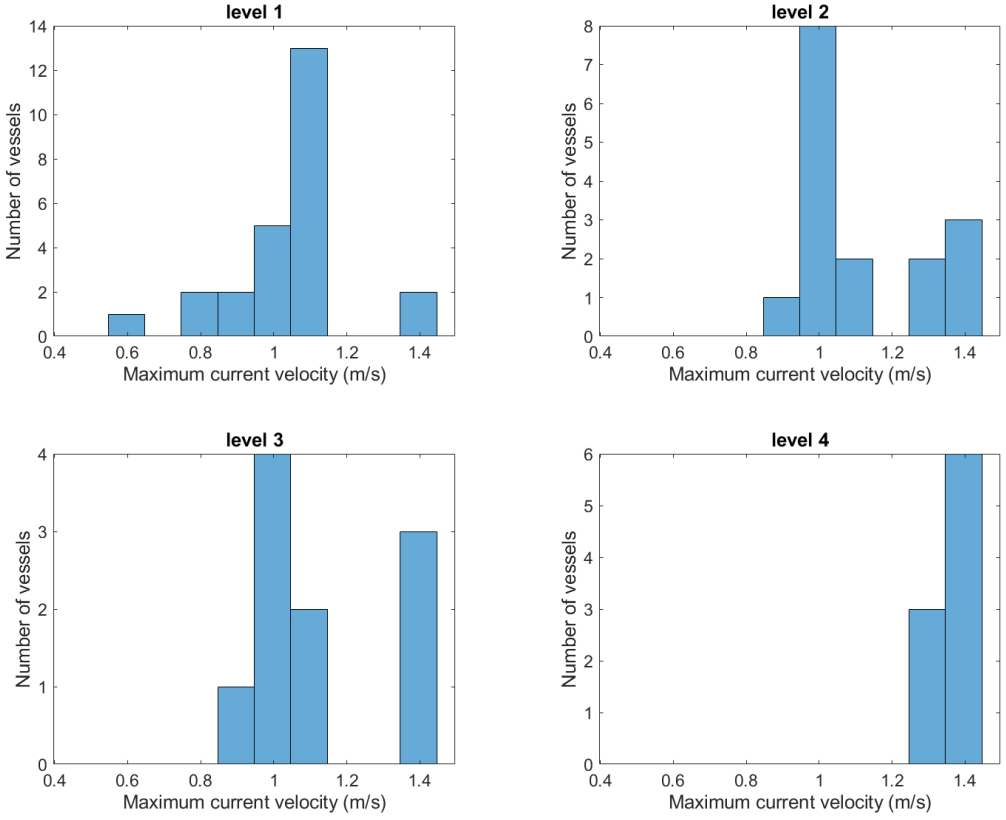

Figure 5.9. Number of damaged vessels for different maximum current velocity ranges based on damage level

While constructing these histograms, the biggest difficulty is the lack of sufficient number of data. For example, for some ranges of water elevations, there are no damaged or washed away vessels. Furthermore, there are some data ranges that neither water elevation nor current velocity is contributing. In order to avoid the errors that could be resulted from these facts, the points are eliminated in the further analyses.

5.3.3. Damage Ratio

The ratio of the vessels damaged or washed away to the total number of vessels for each data range is called D_1 and determined using Eq. 5.1 with the same method of Suppasri et al., (2014).

$$D_1 = \frac{A + B}{A + B + C} \quad [5.1]$$

A = number of vessels that were washed away

B = number of vessels that were damaged (minor, moderate or major)

C = number of vessels that survived

Another damage ratio D_2 is calculated by adapting the method of Aketa et al., (1994, as cited in Suppasri et al., 2014) with Eq. 5.2 after more detailed classification of the damages are performed. This ratio is defined as the weighted damage ratio since it includes constants to reduce impact of minor and moderate damages in the ratio.

$$D_2 = \frac{a + b + 0.5c + 0.25d}{a + b + c + d + e} \quad [5.2]$$

a = number of vessels that were washed away

b = number of vessels that had major damage

c = number of vessels that had moderate damage

d = number of vessels that had minor damage

e = number of vessels that were not damaged

Damage ratio D_1 and the weighted damage ratio D_2 are calculated and plotted against computed maximum water elevation and maximum current velocity to have a better understanding of the effect of tsunami parameters. Figure 5.10 shows the relationship

of damage ratio with the water elevations and current velocities. It can be seen that damage is almost negligible especially for currents smaller than 1 m/s. Although there is not a similar sharp relation for the tsunami height, the trend shows us a general increasing trend of damage ratio with the water elevation. Noting that there are other variables that may have a strong impact on damage (such as vessel weight), we aim to clarify such relationships in the next sections with the help of statistical analysis and fragility functions.

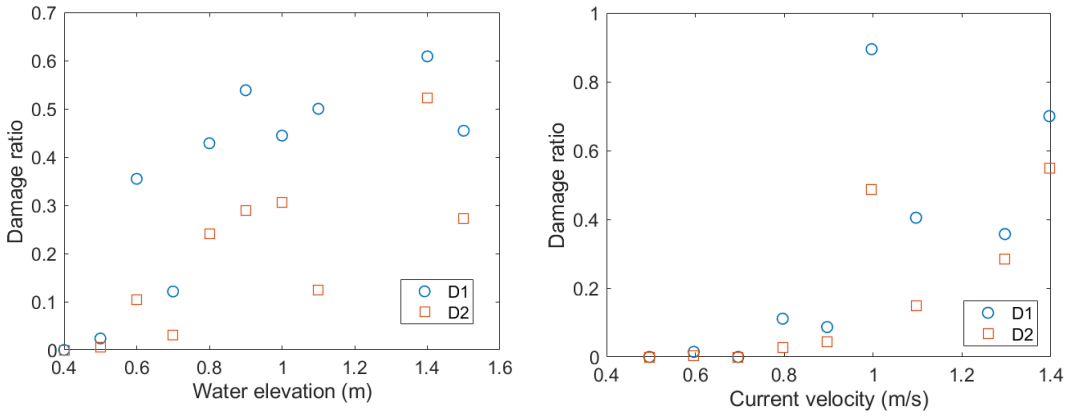

Figure 5.10. Damage ratios for respective tsunami height (left) and current velocity (right)

CHAPTER 6

ESTIMATION OF FRAGILITY FUNCTIONS

Altough some methods used in the field indicates a direct relationship between tsunami intensity and vulnerability, the more reliable methods for estimating vulnerability study the damage state independent from the losses due to that damage level (Charvet et al., 2017). Thus, to describe vulnerability, tsunami intensity measures that relates the model to the damage state are selected. Tsunami intensity measures for this study are chosen as maximum water level (tsunami height) and maximum current velocity (tsunami velocity) in the previous chapters.

6.1. Estimating Probability of Tsunami Damage on Marine Vessels

The aim of this study is to provide fragility functions that determines the probability of occurrence or exceedance of a certain damage level by statistical analysis. To obtain a probability density function, expressing the probability of reaching or exceeding of a certain damage level is needed (Charvet et al., 2013). By definition this probability can be expressed as,

$$p(dl \geq DL_i) = \frac{\sum_i^N v_i}{V} \qquad [6.1]$$

Where DL is the predefined damage level, v is the number of vessels contribute to each damage level, *N* is the number of damage levels, and *V* is the number of vessels included in the analysis.

When expressing the damage level as a function of the tsunami intensity measure, the probability of occurrence or exceedance should be defined for the related measure. Thus, the number of vessels for each damage level should be split according to the range of intensity measure.

The first tsunami intensity measure calculated was maximum water elevation. Therefore, it is started by dividing the maximum water elevation data into bins by 0.1 m increments in the data. Then Eqn. 6.1 can help to calculate the probabilities for each range by considering the data of vessels in each bin separately.

After finding the occurrence or exceedance probability for each damage level, probability is plotted against the mean value of the water elevation at each bin. As mentioned in the Chapter 5, due to lack of sufficient data, there were ranges of water elevation data with no contributing number of damaged vessels. In addition, for some ranges of water elevation there were no simulated data at any of berthing places. When fitting the lognormal curves to each damage level, the missing points are eliminated. The resulting plot is shown in the figure 6.1. Using the same method, also for ranges of current velocity, probability of occurrence of each damage level is plotted (Fig. 6.2). It should be noted that, the fitted curves are not obtained by regression analysis and the plot is not a cumulative density function. Thus, the curves in Figure 6.1 and Figure 6.2 are not a fragility curves. However, it still shows the clear trend between damage levels and water elevation. Another thing to be noted here is that the outliers within the data are not removed or modified. Therefore, errors may be expected.

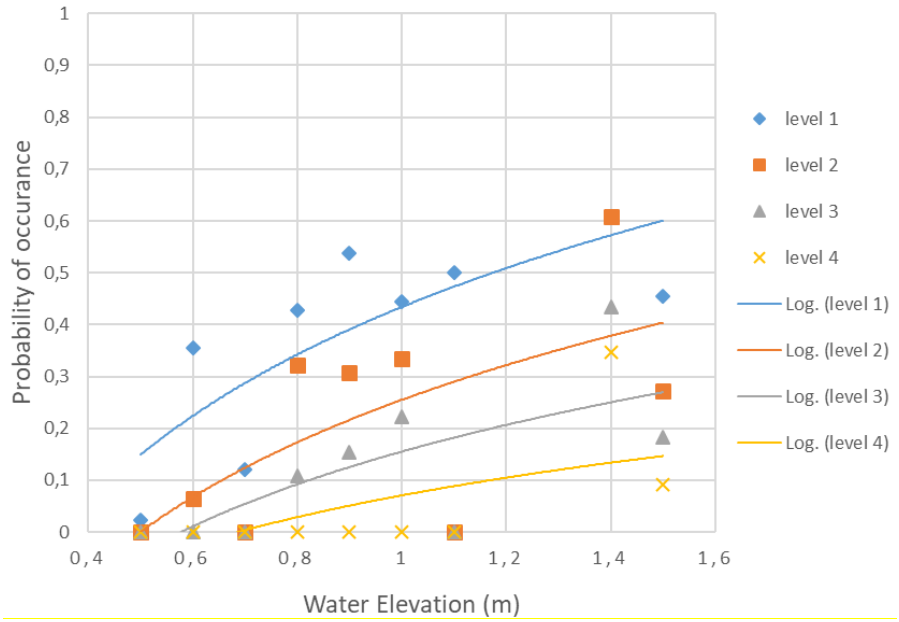

Figure 6.1. Weighted probabilities of damage levels for different water elevations

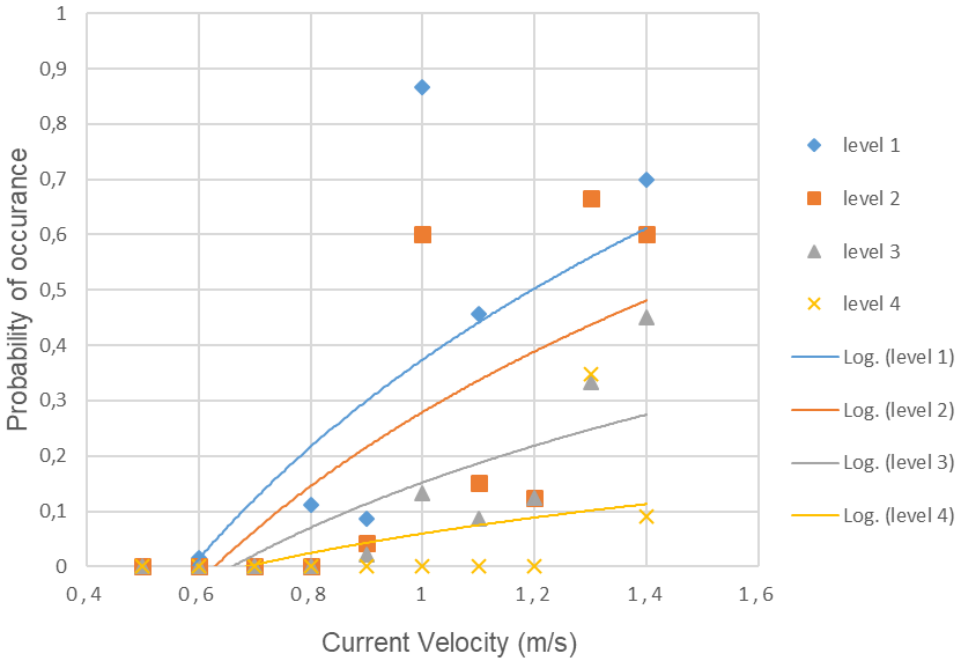

Figure 6.2. Weighted probabilities of damage levels for different current velocities

To validate the usage of bins for tsunami intensity measure, the curves are plotted using the scattered data without using the ranges of water elevation or current velocity (Fig 6.3 and Fig 6.4). It can be seen that the probabilities are same for both curves regardless of using range bins.

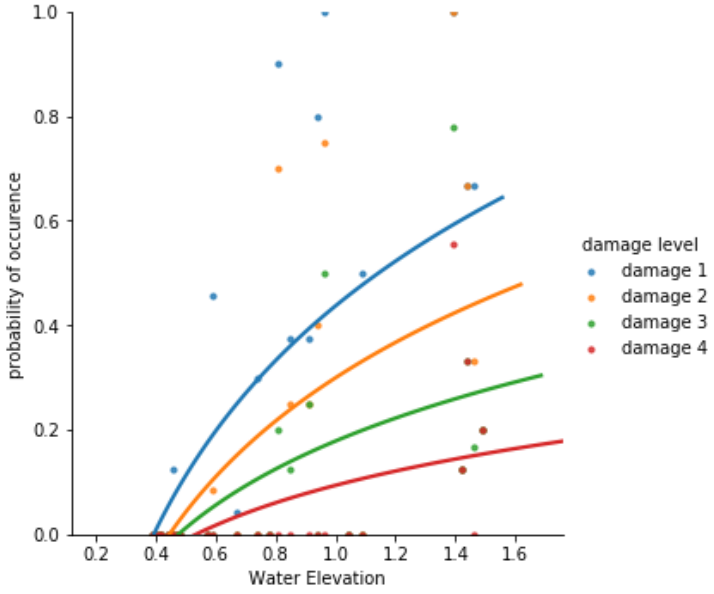

Figure 6.3. Probability of occurrence of damage levels for water elevation

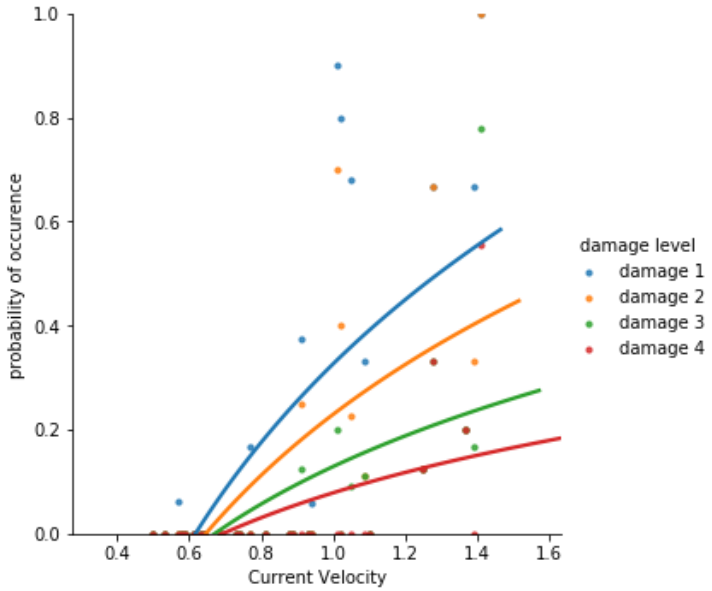

Figure 6.4. Probability of occurrence of damage levels for current velocity

6.2. Regression Analysis

To obtain the fragility curves; the data of the chosen tsunami intensity measures, the data of damage of the vessels and a statistical model that describes the relationship between these two parameters is needed. The statistical model is often a regression model provides the mean and standard deviation of the intensity measure (i.e., water elevation, current velocity) for a given response (i.e., damage level) within a certain error limit. However, the prediction of the probability of damage will be highly dependent on the quality of the dataset, and the suitability of the statistical method used. In order to make reliable damage prediction by fragility curves, correlated error for the regression method should be as small as possible. Therefore, it is necessary to carry out a number of verifications to ensure the smallest error possible for the available data.

For the probability function given in Eq. 6.1, if the response (damage level) is assumed to be a function of the tsunami parameter again, the standard normal cumulative probability function is expressed as;

$$P(X) = \phi\left[\frac{X-\mu}{\sigma}\right] \quad [6.2]$$

$$X = \sigma\phi^{-1} + \mu \quad [6.3]$$

Where X is the tsunami intensity measure, μ is mean of X and σ is the standard deviation of X.

The log-normal cumulative function is;

$$P(X) = \phi\left[\frac{\ln X - \mu'}{\sigma'}\right] \quad [6.4]$$

$$\ln X = \sigma'^{\phi^{-1}} + \mu' \quad [6.5]$$

Where μ' and σ' are mean and standard deviation of $\ln X$ respectively.

By carrying out regression analysis for various models, mean and the standard deviation that result in the least amount of error are determined. Table 6.1 shows the errors of regression models for each damage level. Root mean square error (RMSE) for linear regression with intercept and linear terms is found to be most suitable model since it gives the most reasonable RMSE for all damage levels.

Table 6.1. *RMSE values of each damage level for regression models*

The method used		*RMSE when water elevation is predictor*				*RMSE when current velocity is predictor*			
		DL1	DL2	DL3	DL4	DL1	DL2	DL3	DL4
Linear regression	Linear	0.17	0.19	0.13	0.13	0.26	0.21	0.1	0.13
	Interactions linear	0.17	0.19	0.13	0.13	0.26	0.21	0.1	0.13
	Robust linear	0.2	0.23	0.15	0.12	0.24	0.21	0.12	0.12

	Stepwise linear	0.17	0.24	0.13	0.13	0.26	0.21	0.1	0.13
Regression trees	Fine tree	0.24	0.23	0.16	0.12	0.33	0.29	0.16	0.12
	Medium tree	0.24	0.23	0.16	0.12	0.33	0.29	0.16	0.12
	Coarse tree	0.24	0.23	0.16	0.12	0.33	0.29	0.16	0.12
Support Vector Machines	Fine Gaussian	0.22	0.19	0.14	0.11	0.31	0.28	0.15	0.11
	Medium Gaussian	0.19	0.19	0.13	0.13	0.26	0.27	0.13	0.12
	Coarse Gaussian	0.20	0.22	0.14	0.13	0.3	0.26	0.12	0.11

After selecting the most suitable model as linear regression, the errors need to be examined further since there are important assumptions to be validate in linear regression concept (Charvet et al., 2013). (i), linear regression assumes the difference between the model and the data is normally distributed. (ii), the errors are assumed to have a zero mean. (iii), the errors have a constant variance. (iv), there assume to be no dependency between errors. To increase the prediction quality, these assumptions needs to be checked. Figure 6.5 shows the response and residual plots of the linear regression analysis.

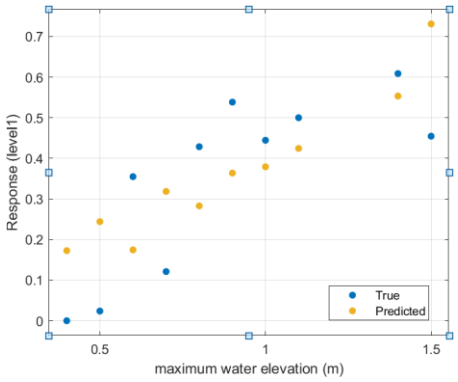
Response (level1)
maximum water elevation (m)
True
Predicted

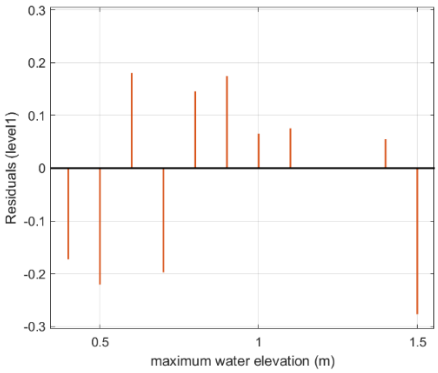
Residuals (level1)
maximum water elevation (m)

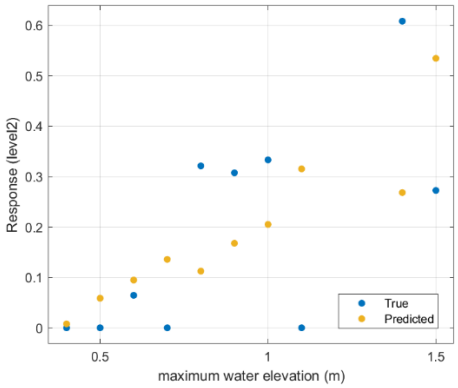
Response (level2)
maximum water elevation (m)
True
Predicted

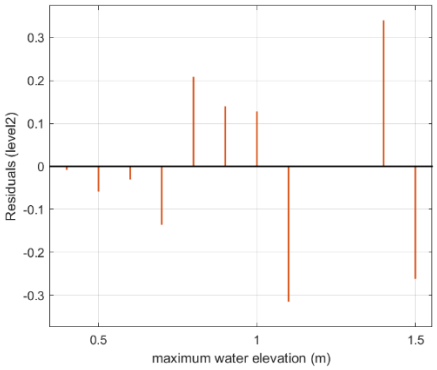
Residuals (level2)
maximum water elevation (m)

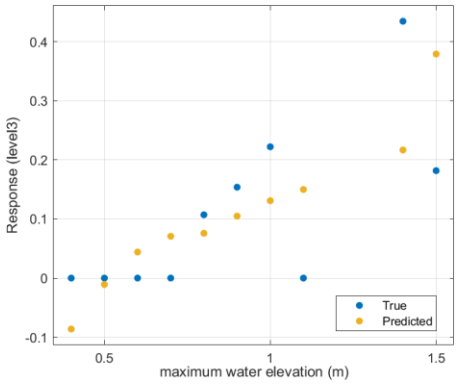
Response (level3)
maximum water elevation (m)
True
Predicted

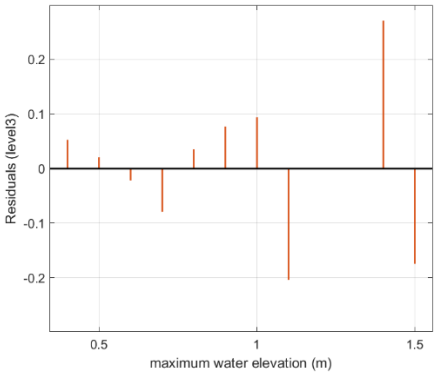
Residuals (level3)
maximum water elevation (m)

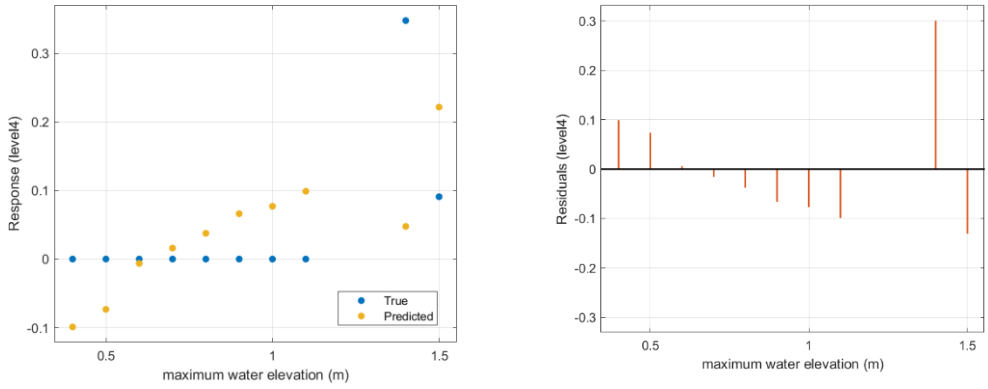

Figure 6.5. Response and residual plots of linear regression analysis for each damage level

After training the data set with linear regression, the model creates predictions for the response value (i.e. damage levels) for a given predictor (i.e. water elevation). By plotting predicted responses in the same graph with the true data contributing to predictor, response plot is obtained. The difference between predicted and true data (linear distance of two points in the plot) defines the error of model. Residual values are simply the error values of predicted response and explain the behavior of the error of the fitted curves. Thus, residual plot can be used to validate the error assumptions given above. For the plots in Figure 6.5, it can be concluded that the error distribution is normal and verifies the first assumption. Secondly, for all damage levels, the mean of residual value in the plot is set as zero. Therefore, assumption (ii) is also satisfied. On the other hand, it can be seen from the residuals plot that the errors are not independent; in fact, a trend between errors exists for all damage levels except damage level 1. In addition, errors may not have a constant variance and the assumption (iii) may not be satisfied because of missing data at some ranges of water elevation.

To overcome these difficulties, a modification in the regression model has been needed. For such cases, Charvet et al., (2013) propose to use of Generalized Linear Model, a method of logistic regression. Generalized Linear Model is favored for our case since it provides a connection to the nature of damage level concept. Moreover, it considers the weighted distribution of data points and prevents the overestimations

due to lack of data. In the model, maximum likelihood estimation is applied to find the best fit to the response variable.

When applying this method, it should be taken into consideration that the damage level data is discrete. In addition, there is an order in the intensity of the damage levels, thus, the response needs to be defined as ordinal. As a result, ordinal scale must be used. If we apply the definition of ordinal response from Mc Cullagh & Nelder, (1989) to vessel fragility due to tsunami, we can list the conditions of ordinarity as follows. (i) Each damage level must express a different intensity of the response by an increasing or decreasing order. (ii) Damage levels must be mutually exclusive. The first requirement is satisfied by the nature of damage level scale. However, damage level 4 mentioned in our study is the condition of a vessel being washed away. This condition doesn't necessarily exclusive from other damage levels by nature. Therefore, to obtain a reliable fragility curve, damage level 4 needs to be excluded from the data. Otherwise, there can be an unreasonable outcome for the level 4 curve.

6.3. Fragility Curves

Fragility curves are, basically, cumulative distribution curves that gives the relationship of occurrence or exceedance of a damage level to marine vessel over a range of tsunami intensity measure (e.g., water elevation) (Dias & Edirisooriya, 2019). Each individual curve represents the exceedance of a certain damage category. In our case these categories are damage levels assigned for the conditions of the vessels as survived, minor, moderate of major damaged and washed away.

The methodology of the regression analysis and the reasons to choose the given regression model are explained in the previous section. As a result, a generalized linear model is applied considering ordinal regression and the best fit is found by maximum likelihood estimation. Fig. 6.6 shows the fragility curves assuming log-normal distribution of the data including all of the damaged vessels for water elevation and current velocity.

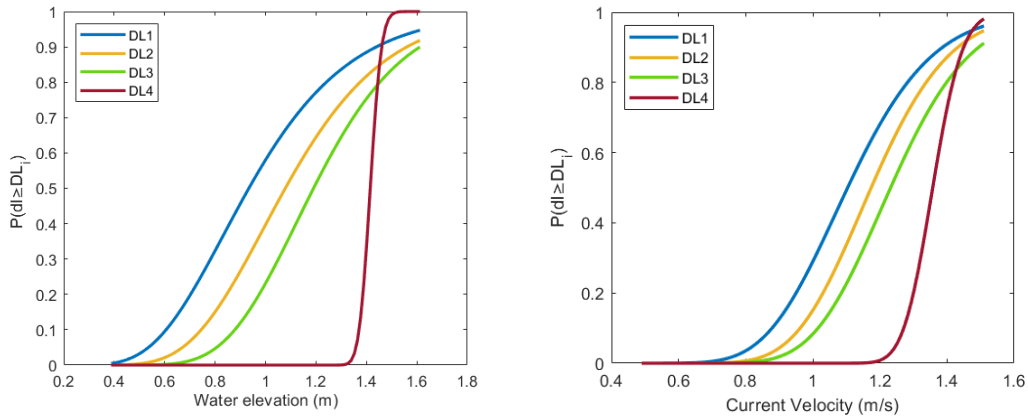

Figure 6.6. Fragility curves of water elevation and current velocity for all damaged vessels

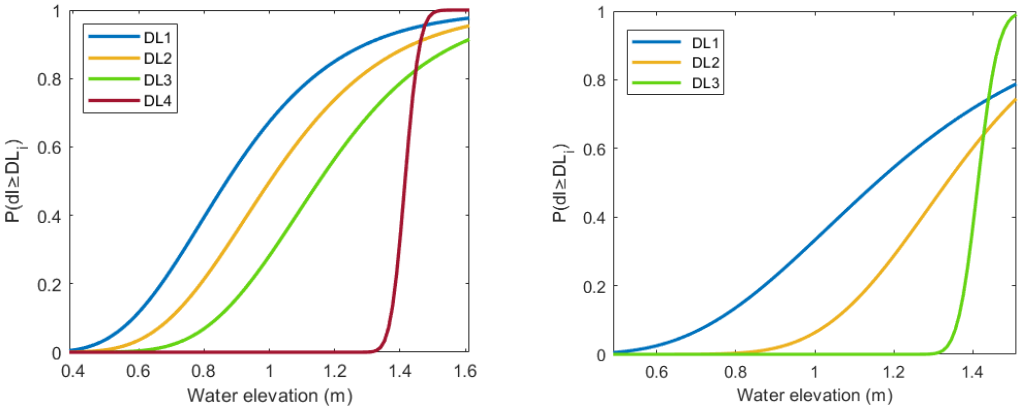

Figure 6.7. Fragility curves of water elevation for vessel materials (i) fiber; (ii) wood

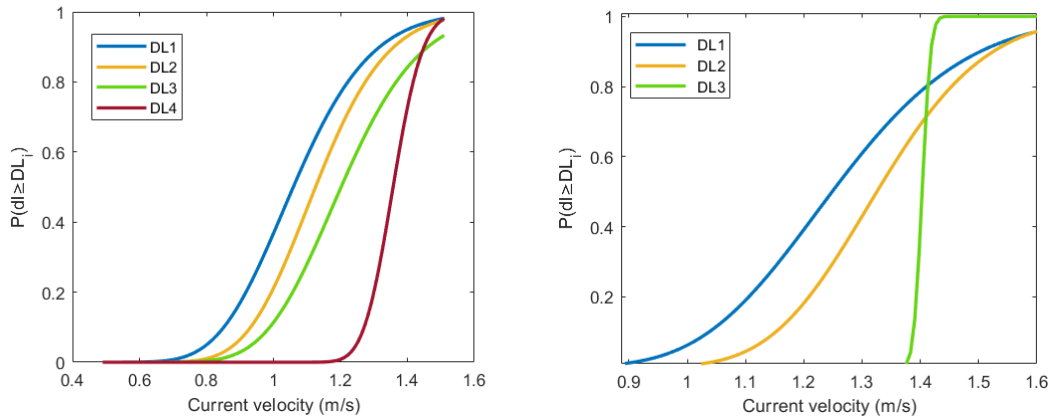

Figure 6.8. Fragility curves of current velocity for vessel materials (i) fiber; (ii) wood

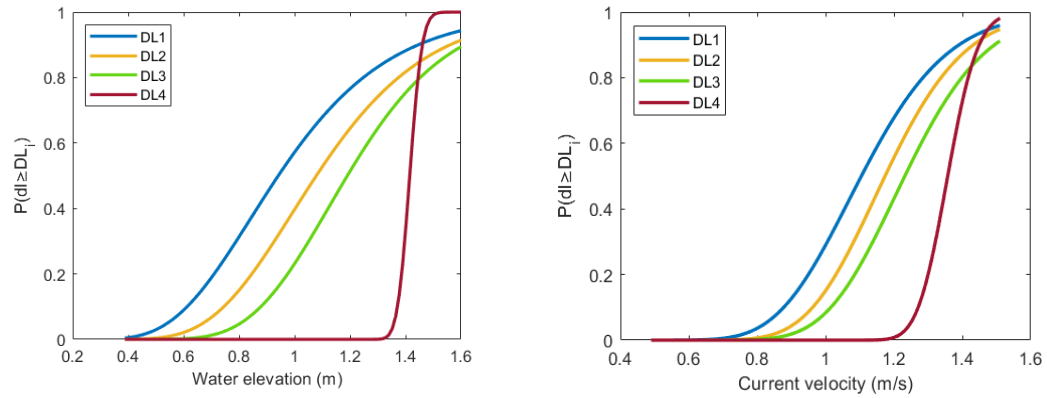

Figure 6.9. Fragility curves of water elevation and current velocity for damaged vessels smaller than 5 tons

The mean and standard deviation values for the occurrence of level 3 damage is driven from the fragility curves in Figures 6.6-6.9 and given in the Table 6.2. Since the most loss is always associated with the highest damage level, the damage level that results in a complete loss used as the most explanatory level to define damage in the literature. In Gumbet Bay case, even though level 4 damage is considered to happen when the tsunami intensity measures higher compared to other levels, it cannot be used as an explanatory level of damage. This is partly because of the definition of washed away

vessels, it may not express a greater loss than major damage (level 3). Nonetheless, the main reason is the lack of sufficient number of data points akin to level 4 damage. In addition, as stated in Chapter 5, for the experienced tsunami, there were no damage levels that caused a complete loss in Gumbet Bay. As a result of fact, damage level 3 (major damage) considered as a sufficient indicator of fragility for vessels at the Gumbet Bay. Therefore, mean values of water elevation and current velocity in Table 6.2 can be referred as the conditions for the occurrence of major damage.

Table 6.2. *The values of mean and standard deviation for Damage Level 3*

Vessel properties	*Water elevation*		*Current velocity*	
	μ'	σ'	μ'	σ'
All vessels	1.224	0.294	1.246	0.189
Wooden	1.413	0.040	1.403	0.011
Fiber	1.188	0.296	1.216	0.186
≤5t	1.224	0.294	1.246	0.189

For wooden vessels, when the water elevation reaches around 1.4 m or the current velocity reaches 1.4 m/s major damage is expected to occur. On the other hand, these numbers a relatively smaller for the vessels produced by fiber materials such as 1.2 m and 1.2 m/s respectively. This may be caused by the difference of material densities since the material density is a compound of the vessel weight and the buoyancy force. Thus, it can be deducted that for two vessels with same size, the one produced by a denser material will yield a less probability of fragility.

There was almost no damage observed for vessels larger than 5 tons within the experienced range of tsunami parameters. Therefore, almost all of the damaged vessels shown in fragility curves are smaller than 5 tons. As a result of this, it can be indicated that for tsunamis producing water elevations and currents smaller than 1.5

m and 1.4 m/s respectively, vessels bigger than 5 tons are hardly expected to experience any damage. And major damage is expected for vessels smaller than 5 tons for tsunamis producing water elevations and currents larger than 1.2 m and 1.2 m/s.

6.4. Interpreting Tsunami Fragility Curves with SHAP

In the case of creating fragility curves with small set of data, understanding the nature of variables may help to explain why the statistical models used made certain predictions. Fragility curves are developed to predict damage for a given tsunami intensity measure and improve risk mitigation strategies. Thus, before acting based of the fragility curve obtained by a specific statistical model, it is more crucial to comprehend behavior of the dataset and interpreting it.

A recently proposed method by Lundberg & Lee, (2017) that unifies six existing methods; SHAP (SHapley Additive exPlanations) is selected for the interpretation of the dataset prepared. SHAP is easy to understand since it assigns each feature in the dataset an impportance value for prediction (damage level for our case) and shows better consistency with human intuition than previous approaches (Lundberg & Lee, 2017).

SHAP framework available in the library of Python software is used in the computations and visually explain the following computations. The source code of the SHAP used in Python can be obtained from https://github.com/slundberg/shap.

The abbreviations used for the properties in the code; size is vessel length (m), maxTsuH is maximum water elevation (m) and maxTsuVel is maximum current velocity (m/s) obtained from NAMI DANCE, tonnage is vessel weight in tons, material_f and material_w are respectively fiber and wooden vessels.

After training the data in SHAP method, mean error of the model is found as 0.13. SHAP calculates variable called SHAP value for each feature of the dataset based on the impact of that feature on the prediction of response value. Figure 6.10 shows that

the decrease in the values of vessel length, water elevation and current velocity results in smaller SHAP values.

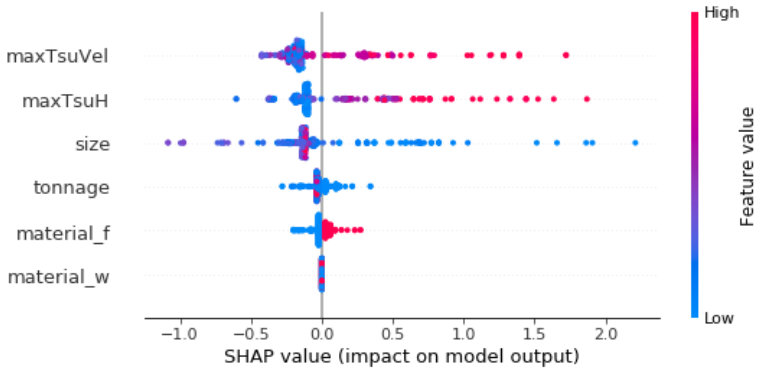

Figure 6.10. Impact of model output

Figure 6.11 shows the F score of each feature. F score is a feature of SHAP algorithm that scores the parameters in the dataset according to their impact on response value. It can be seen that size of the vessel is a governing feature and in more coherence with the tsunami damage on vessels.

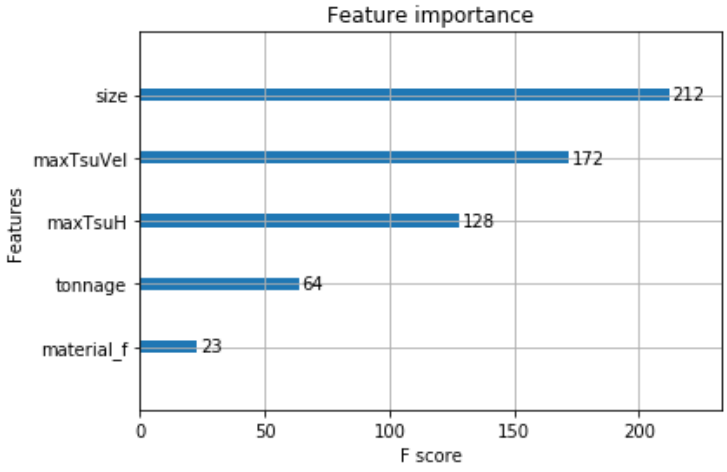

Figure 6.11. Feature importance of the tsunami and vessel parameters according to their impact on damage level

Figure 6.12 and 6.13 presents the heatmaps, the multivariate relationship of the vessel weight and tsunami intensity measures (respectively, maximum water elevation and current velocity) to the damage level.

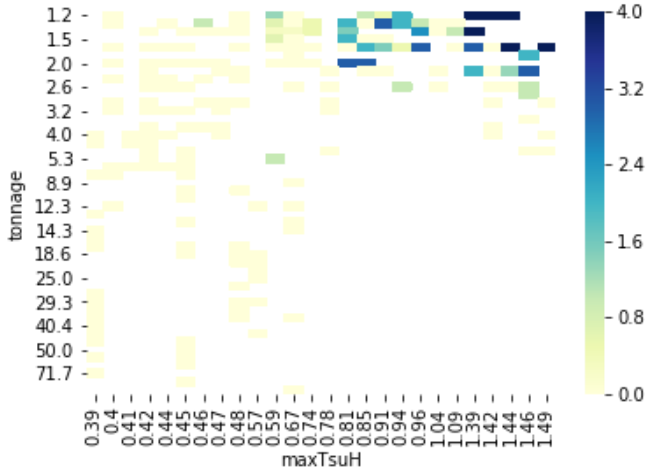

Figure 6.12. Heatmap of the vessel weight and maximum water elevation on damage

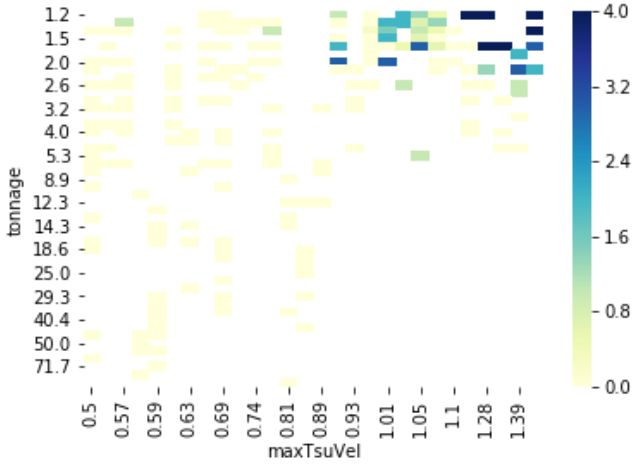

Figure 6.13. Heatmap of the vessel weight and maximum current velocity on damage

CHAPTER 7

CONCLUSION

In this study, tsunami damage of marine vessels in Gumbet Bay due to Bodrum-Kos tsunami is investigated by developing fragility functions based on the vessel material and vessel weight. Since fragility curves depend on the reliable dataset and suitable regression method, validations are done for every step when generating data and choosing the proper statistical method.

First of all, numerical simulations are done with three different source models. In fact, south dipping and north dipping plane source models resulted in accordance with the observed water elevations and current velocities quantitatively. However, for qualitative measures like arrival time of the first wave or duration of shoreline withdrawal, elliptic source produced more accurate waves. Therefore, the results of the elliptic source model are decided to be used in the fragility analysis. Secondly, the number of vessels are obtained by examination of satellite images taken from Google Earth and properties such as production material and vessel length and vessel weight is determined. In summary, 305 vessels are included in the study, with 47% of them classified as fiber and %53 of them classified as wooden. 75% of the vessels were small marine vessels weighting less than 5 tons. After then, 5 different damage categories are decided to be used for classification of the state of damage. There are no damage categories that correspond to total loss unlike the fragility functions developed for 2004 Indian Ocean tsunami and 2011 Great East Japan tsunami. This is mainly because of the fact that Bodrum-Kos tsunami is far less strong than the other two catastrophic tsunamis mentioned. After all, the damage levels are assigned for survived, minor damaged, moderate damaged, major damaged and washed away vessels are level 0, level 1, level 2, level 3 and level 4 respectively. Washed away vessels are assigned as level 4 since the state is assumed to happen for higher values

of water elevation and current velocity. After the first analysis, as expected, the values of water elevation and current velocity of the waves that hit to points where the washed away vessels are found considerably higher. Lastly, a dataset is prepared for 305 vessels including information of the tsunami parameters that hit to vessel (water elevation and current velocity), vessel properties (material, length and weight), the berthing place vessel was moored, the depth of the vessels' location before tsunami and damage level of the vessel after tsunami. After the obtaining reliable dataset, first compound of the fragility curves, next step was determination of suitable statistical analysis method. To begin with, for the ease of calculation and to avoid errors related to usage of limited number of data, water elevation and current velocity is divided into small bins with 0.1 unit increments. The probability of occurrence of a given damage level for a value of tsunami parameter is weighted according to the number of vessels in that bin. This approach helped to avoid over estimation of damage and gives a rough relationship between the tsunami intensity measure and the level of damage. However, it cannot provide us fragility curve. Next, a few number of regression models are used to find a suitable statistical model with least error. A code is developed and machine learning tools in MATLAB software is used to train data for numerous models and linear regression model with least square fit is found to be least erroneous. In spite of resulting the least error, the quality of the model cannot be guaranteed without validation of the suitability of the dataset. For this, the conditions to satisfy a linear regression criterion are checked. Due to lack of data points, the distribution of data failed to satisfy requirement of linear regression method. This was another expected outcome when working with insufficient number of data. The fragility studies that use linear least squares regression often includes large number of data points up to many hundreds. To overcome this challenge, regression method is modified with the generalized linear model, a logistic regression model that uses ordinal regression with maximum likelihood estimation to obtain best fit. Nonetheless, another problem is faced when using the generalized linear model. In order to satisfy ordinal regression definition, the damage levels should be mutually exclusive and in an order of increasing intensity. On the other hand, although damage level 4 in our case

corresponds to washed away vessels and occurs for higher values of tsunami intensity measures, it is not necessarily results in larger loss and not mutually exclusive from the other damages by its nature. Therefore, errors related to damage level 4 are expected. Finally, fragility curves are plotted and mean and standard deviation of these curves are given for damage level 3. Even though level 4 curves stated to be prone to overestimation, they are included in the analysis for two reasons; to keep a sufficient number of data, and to show the behavior of level 4 curves.

In summary, it is found out in this study that for wooden vessels smaller than 5 t, major damage is expected when the water elevation reaches around 1.4 m or the current velocity reaches 1.4 m/s. For fiber vessels smaller than 5 t, these water elevation and current velocity values become 1.2 m and 1.2 m/s respectively. This may be caused by the difference of material densities since the material density is a compound of the vessel weight and the buoyancy force. Thus, it can be deducted that for two vessels with same size, the one produced by a denser material would yield less fragility. For vessels larger than 5t tons, major damage is not expected for water elevations and currents smaller than 1.5 m and 1.4 m/s respectively.

Fragility curves developed for the vessels damaged by Bodrum-Kos tsunami show a strong relation between fragility and the vessel properties. Therefore, it can be concluded that, fragility functions strongly depend on the area they are developed for. In other words, for the same values of tsunami intensity measures (such as water elevation and current velocity), two different losses can be expected from two different regions depending on the vessel properties that are commonly used and govern in the region. Another point to be considered is the impact of human response to tsunami fragility of the vessels. In case of Gumbet Bay, tsunami occurred after midnight when all the boats were berthed, and the arrival time of the tsunami was not sufficient enough for seamen to realize a tsunami was coming. Moreover, seamen in the Gumbet Bay was not aware of tsunami risk in the region. Therefore, there were no significant human response to the tsunami in this case which also emphasizes the necessity of increasing tsunami awareness in such areas.

This study is a first step taken to calculate probabilities of tsunami related losses in Bodrum region. In further studies, more detailed and region specific loss functions can be developed to estimate the financial loss with the help of more available data and information on economic losses due to such kind of hazards. These studies will help increasing tsunami preparedness and quick recovery.

REFERENCES

Admire, A. R., Dengler, L. A., Crawford, G. B., Uslu, B. U., Borrero, J. C., Greer, S. D., & Wilson, R. I. (2014). Observed and Modeled Currents from the Tohoku-oki, Japan and other Recent Tsunamis in Northern California. *Pure and Applied Geophysics*, *171*(12), 3385–3403. https://doi.org/10.1007/s00024-014-0797-8

AFAD(Disaster and Emergency Management Presidency Earthquake Department). (2017). *July 21th 2017 Bodrum Offshore Earthquake*.

Aketa, S., Yano, K., Mizuno, Y., Sato, J., & Terauchi, K. (1994). Re-duction effect of port and fishing port facilities by tsunami damage. *Coastal Engineering Conference (JSCE)*, 1176–1180. Tokyo: Japan Society of Civil Engineers (JSCE).

Altinok, Y., Alpar, B., Özer, N., & Aykurt, H. (2011). Revision of the tsunami catalogue affecting Turkish coasts and surrounding regions. *Natural Hazards and Earth System Science*, *11*(2), 273–291. https://doi.org/10.5194/nhess-11-273-2011

Altinok, Y., Alpar, B., Özer, N., & Gazioglu, C. (2005). 1881 and 1949 earthquakes at the Chios-Cesme Strait (Aegean Sea) and their relation to tsunamis. *Natural Hazards and Earth System Science*, *5*(5), 717–725. https://doi.org/10.5194/nhess-5-717-2005

Altınok, Y., & Ersoy, Ş. (2000). Tsunamis Observed on and Near the Turkish Coast. *Natural Hazards*, *21*(2), 185–205. https://doi.org/10.1023/A:1008155117243

Ambraseys, N. N. (1960). The seismic sea wave of July 9, 1956, in the Greek archipelago. *Journal of Geophysical Research*, *65*(4), 1257–1265. https://doi.org/10.1029/JZ065i004p01257

Ambraseys, N. N. (1962). Data for the investigation of the seismic sea-waves in the Eastern Mediterranean. *Bulletin of the Seismological Society of America*, *52*(4), 895–913.

Antonopoulos, A. (1978). Contribution to the knowledge of tsunamis in the Eastern Mediterranean from ancient times until the recent. *Annales Geology Pays Hellenic*, *29*(2), 740–757.

Batıgün, E., Yolsal-çevikbilen, S., & Taymaz, T. (2018). Source Characteristics of 2017 Ayvacik , Lesvos , and Bodrum-Kos Earthquakes Obtained from Regional Moment Tensor Inversion. In *EGU2018-761, Geophysical Research Abstracts, Vol. 20, Poster*, (Vol. 20). Vienna, Austria.

Beisel, S., Chubarov, L., Didenkulova, I., Kit, E., Levin, A., Pelinovsky, E., …

Sladkevich, M. (2009). The 1956 Greek tsunami recorded at Yafo, Israel, and its numerical modeling. *Journal of Geophysical Research*, *114*(C9), C09002. https://doi.org/10.1029/2008JC005262

Cakir, T. E., & Yalciner, A. C. (2002). Effects of 1956 South Aegean tsunami to Bodrum Peninsula. *Turkish Chamber of Civil Engineers 4th National Coastal Engineering Symposium*. Antalya.

Charvet, I., Macabuag, J., & Rossetto, T. (2017). Estimating tsunami-induced building damage through fragility functions: Critical review and research needs. *Frontiers in Built Environment*, *3*(August). https://doi.org/10.3389/fbuil.2017.00036

Charvet, I., Suppasri, A., Imamura, F., & Rosetto, T. (2013). Comparison between linear least squares and GLM regression for fragility functions: example of the 2011 Japan tsunami. *Proceedings of International Sessions in Coastal Engineering, JSCE*, *4*.

De Risi, R., Goda, K., Yasuda, T., & Mori, N. (2017). Is flow velocity important in tsunami empirical fragility modeling? *Earth-Science Reviews*, *166*, 64–82. https://doi.org/10.1016/j.earscirev.2016.12.015

Dias, W. P. S., & Edirisooriya, U. (2019). Derivation of tsunami damage curves from fragility functions. *Natural Hazards*, *96*(3), 1153–1166. https://doi.org/10.1007/s11069-019-03601-8

Dogan, G. G., Annunziato, A., Papadopoulos, G. A., Guler, H. G., Yalciner, A. C., Cakir, T. E., … Synolakis, C. (2019). The 20th July 2017 Bodrum–Kos Tsunami Field Survey. *Pure and Applied Geophysics*, *176*(7), 2925–2949. https://doi.org/10.1007/s00024-019-02151-1

Durran, D. R. (1999). *Numerical Methods for Wave Equations in Geophysical Fluid Dynamics*. New York, Berlin: Springer-Verlag.

Galanopoulos, A. G. (1957). The seismic sea-wave of 9 July 1956. *Praktika Academy*, *32*, 90–101.

Ganas, A., Elias, P., Valkaniotis, S., Briole, P., Kapetanidis, V., Kassaras, I., … Moshou, A. (2017). Co-seismic deformationand preliminary fault modelof the July20, 2017 M6.6Kos earthquake, Aegean Sea. *Aegean Sea Report, EMSC*. https://doi.org/10.13140/RG.2.2.33057.30564

Gica, E., Spillane, M. C., Titov, V. V., Chamberlin, C. D., & Newman, J. C. (2008). *Development of the forecast propagation database for NOAA's Short-Term Inundation Forecast for Tsunamis (SIFT)*. 95.

Goto, C., & Ogawa, Y. (1997). Numerical Method of Tsunami Simulation with the Leap-Frog Scheme. *IOC Manuals and Guides No. 35*.

Hathaway, Q. A., Roth, S. M., Pinti, M. V., Sprando, D. C., Kunovac, A., Durr, A. J.,

… Hollander, J. M. (2019). Machine-learning to stratify diabetic patients using novel cardiac biomarkers and integrative genomics. *Cardiovascular Diabetology*, *18*(1), 78. https://doi.org/10.1186/s12933-019-0879-0

Imamura, F. (1989). *Tsunami Numerical Simulation with the Staggered Leap-Frog Scheme (Numerical Code of TUNAMI-N1).*

Imamura, F. (1996). Review of Tsunami Simulation with a Finite Difference Method. In H. Yeh, P. Liu, & C. Synolakis (Eds.), *LongWave Runup Models* (pp. 25–42). Singapore: World Scientific Publishing Co Pte Ltd.

Imamura, F., Yalçıner, A. C., & Özyurt, G. (2006). *TUNAMI N2 Tsunami modeling manual.*

Karasözen, E., Nissen, E., Büyükakpinar, P., Cambaz, M. D., Kahraman, M., Ertan, E. K., … Özacar, A. A. (2018). The 2017 July 20Mw 6.6 Bodrum-Kos earthquake illuminates active faulting in the Gulf of Gökova, SW Turkey. *Geophysical Journal International*, *214*(1), 185–199. https://doi.org/10.1093/gji/ggy114

Kiratzi, A., & Koskosidi, A. (2018). Constrains on the Near-Source Motions of the Kos-Bpdrum 20 July 2017 Mw 6.6 Earthquake. *16th European Conferance on Eartquake Engineering*, (July), 8–13. Thessaloniki, Greece.

Kitsantonis, N. (2017). Earthquake in Aegean Sea Kills 2 Tourists. *The New York Times*.

KOERI (Kandilli Observatory and Earthquake Research Institute). (2017). *Report of 21 July 2017 Gokova Bay - Mediterranean Earthquake distributed by KOERI Regional Earthquake and Tsunami monitoring Center (in Turkish).*

Koshimura, S., Namegaya, Y., & Yanagisawa, H. (2009). Tsunami Fragility — A New Measure to Identify Tsunami Damage —. *Journal of Disaster Research*, *4*(6), 479–488. https://doi.org/10.20965/jdr.2009.p0479

Lundberg, S. M., & Lee, S. I. (2017). A unified approach to interpreting model predictions. *Advances in Neural Information Processing Systems*.

Lynett, P. J., Borrero, J. C., Weiss, R., Son, S., Greer, D., & Renteria, W. (2012). Observations and modeling of tsunami-induced currents in ports and harbors. *Earth and Planetary Science Letters*, *327–328*, 68–74. https://doi.org/10.1016/j.epsl.2012.02.002

Lynett, P. J., Borrero, J., Son, S., Wilson, R., & Miller, K. (2014). Assessment of the tsunami-induced current hazard. *Geophysical Research Letters*, *41*(6), 2048–2055. https://doi.org/10.1002/2013GL058680

Lynett, P. J., Gately, K., Wilson, R., Montoya, L., Arcas, D., Aytore, B., … Zhang, Y. J. (2017). Inter-model analysis of tsunami-induced coastal currents. *Ocean*

Modelling, *114*, 14–32. https://doi.org/10.1016/j.ocemod.2017.04.003

Mc Cullagh, P., & Nelder, J. A. (1989). *Generalized Linear Models* (Second Edi). Chapman & Hall /CRC.

McKenzie, D. (1972). Active Tectonics of the Mediterranean Region. *Geophysical Journal International*, *30*(2), 109–185. https://doi.org/10.1111/j.1365-246X.1972.tb02351.x

Muhari, A., Charvet, I., Tsuyoshi, F., Suppasri, A., & Imamura, F. (2015). Assessment of tsunami hazards in ports and their impact on marine vessels derived from tsunami models and the observed damage data. *Natural Hazards*, *78*(2), 1309–1328. https://doi.org/10.1007/s11069-015-1772-0

Okal, E. A., Fritz, H. M., Raad, P. E., Synolakis, C., Al-Shijbi, Y., & Al-Saifi, M. (2006). Oman Field Survey after the December 2004 Indian Ocean Tsunami. *Earthquake Spectra*, *22*(S3), 203–218. https://doi.org/10.1193/1.2202647

Okal, E. A., Fritz, H. M., Raveloson, R., Joelson, G., Pančošková, P., & Rambolamanana, G. (2006). Madagascar Field Survey after the December 2004 Indian Ocean Tsunami. *Earthquake Spectra*, *22*(S3), 263–283. https://doi.org/10.1193/1.2202646

Okal, E. A. S., Sladen, A., & Okal, E. A. S. (2006). Rodrigues, Mauritius, and Réunion Islands Field Survey after the December 2004 Indian Ocean Tsunami. *Earthquake Spectra*, *22*(S3), 241–261. https://doi.org/10.1193/1.2209190

Okal, E. A., Synolakis, C. E., Uslu, B., Kalligeris, N., & Voukouvalas, E. (2009). The 1956 earthquake and tsunami in Amorgos, Greece. *Geophysical Journal International*, *178*(3), 1533–1554. https://doi.org/10.1111/j.1365-246X.2009.04237.x

Papadopoulos, G. A., Daskalaki, E., Fokaefs, A., & Giraleas, N. (2007). Tsunami hazards in the Eastern Mediterranean: strong earthquakes and tsunamis in the East Hellenic Arc and Trench system. *Natural Hazards and Earth System Sciences*, *7*(1), 57–64. https://doi.org/10.5194/nhess-7-57-2007

Papadopoulos, G.A., & Chalkis, B. J. (1984). Tsunamis observed in Greece and the surrounding area from antiquity up to the present times. *Marine Geology*, *56*(1–4), 309–317. https://doi.org/10.1016/0025-3227(84)90022-7

Papadopoulos, Gerassimos A. (1993). Seismic faulting and nonseismic tsunami generation in Greece. *IUGG/IOC International Tsunami Symposium*, 115–123. Wakayama, Japan.

Papadopoulos, Gerassimos A., Agalos, A., Charalampakis, M., Kontoes, C., Papoutsis, I., Atzori, S., … Traintafyllou, I. (2019). Fault models for the Bodrum-Kos tsunamigenic earthquake (Mw6.6) of 20 July 2017 in the east Aegean Sea. *Journal of Geodynamics*, 101646. https://doi.org/10.1016/j.jog.2019.101646

Papadopoulos, Gerassimos A., & Pavlides, S. B. (1992). The large 1956 earthquake in the South Aegean: Macroseismic field configuration, faulting and neotectonics of Amorgos Island. *Earth and Planetary Science Letters*, *113*, 383–396.

Papazachos, B. C., Koutitas, C., Hatzidimitriou, P. M., Karacostas, B. G., & Papaioannou, C. (1986). Tsunami hazard in Greece and the surrounding area. *Annales Geophysicae, Series B.*, 79-90.

Pianpanit, T., Lolak, S., Sawangjai, P., Ditthapron, A., & Marukatat, S. (2019). *A comparative study for interpreting deep learning prediction of the*. (August).

Poirier, J. P., & Taher, M. A. (1980). Historical seismicity in the near and middle east, north Africa, and Spain from Arabic documents (VII–XVIIIth century). *Bulletin of the Seismological Society of America*, *70*(6), 2185–2201.

Ribeiro, M. T., Singh, S., & Guestrin, C. (2016). "Why Should I Trust You?" Explaining the Predictions of Any Classifier. *Proceedings of the 22nd ACM SIGKDD International Conference on Knowledge Discovery and Data Mining - KDD '16*, 1135–1144. https://doi.org/10.1145/2939672.2939778

Saltogianni, V., Taymaz, T., Yolsal-Çevikbilen, S., Eken, T., Moschas, F., & Stiros, S. (2017). *Fault-model of the 2017 Kos-Bodrum (east Aegean Sea) Mw 6.6 earthquake from inversion of seismological and GPS data – Preliminary Report*. https://doi.org/0.1785/0120160080.Yal

Shuto, N., Goto, C., & Imamura, F. (1990). Numerical Simulation as a Means of Warning for Near-Field Tsunamis. *Coastal Engineering in Japan*, *33*(2), 173–193. https://doi.org/10.1080/05785634.1990.11924532

Smith, H., & Rourke, A. (2017). Earthquake in Turkey and Greece leaves at least two dead in Kos. *The Guardian*.

Song, J., De Risi, R., & Goda, K. (2017). Influence of flow velocity on tsunami loss estimation. *Geosciences (Switzerland)*, *7*(4). https://doi.org/10.3390/geosciences7040114

Spadon, G., Carvalho, A. C. P. L. F. de, Rodrigues-Jr, J. F., & Alves, L. G. A. (2019). Reconstructing commuters network using machine learning and urban indicators. *Scientific Reports*, *9*(1), 11801. https://doi.org/10.1038/s41598-019-48295-x

Suppasri, A., Koshimura, S., & Imamura, F. (2011). Developing tsunami fragility curves based on the satellite remote sensing and the numerical modeling of the 2004 Indian Ocean tsunami in Thailand. *Natural Hazards and Earth System Science*, *11*(1), 173–189. https://doi.org/10.5194/nhess-11-173-2011

Suppasri, Anawat, Fukui, K., Yamashita, K., Leelawat, N., Ohira, H., & Imamura, F. (2018). Developing fragility functions for aquaculture rafts and eelgrass in the case of the 2011 Great East Japan tsunami. *Natural Hazards and Earth System Sciences*, *18*(1), 145–155. https://doi.org/10.5194/nhess-18-145-2018

Suppasri, Anawat, Mas, E., Koshimura, S., Imai, K., Harada, K., & Imamura, F. (2012). Developing Tsunami Fragility Curves from the Surveyed Data of the 2011 Great East Japan Tsunami in Sendai and Ishinomaki Plains. *Coastal Engineering Journal*, *54*(1), 1250008-1-1250008–1250016. https://doi.org/10.1142/s0578563412500088

Suppasri, Anawat, Muhari, A., Futami, T., Imamura, F., & Shuto, N. (2014). Loss Functions for Small Marine Vessels Based on Survey Data and Numerical Simulation of the 2011 Great East Japan Tsunami. *Journal of Waterway, Port, Coastal, and Ocean Engineering*, *140*(5), 04014018. https://doi.org/10.1061/(ASCE)WW.1943-5460.0000244

Tiryakioğlu, Aktuğ, B., Yiğit, C., Yavaşoğlu, H. H., Sozbilir, H., Özkaymak, … Özener, H. (2018). Slip distribution and source parameters of the 20 July 2017 Bodrum-Kos earthquake (Mw6.6) from GPS observations. *Geodinamica Acta*, *30*(1), 1–14. https://doi.org/10.1080/09853111.2017.1408264

Titov, V., Kânoğlu, U., & Synolakis, C. (2016). Development of MOST for Real-Time Tsunami Forecasting. *Journal of Waterway, Port, Coastal, and Ocean Engineering*, *142*(6), 03116004. https://doi.org/10.1061/(ASCE)WW.1943-5460.0000357

Tselentis, G. A., Stavrakakis, G., Makropoulos, K., Latousakis, J., & Drakopoulos, J. (1988). Seismic moments of earthquakes at the western Hellenic arc and their application to the seismic hazard of the area. *Tectonophysics*. https://doi.org/10.1016/0040-1951(88)90161-8

UNESCO Interational Tsunami Information Center. (n.d.). What is tsunami? Retrieved August 16, 2019, from http://itic.ioc-unesco.org/index.php?option=com_content&view=article&id=1162:what-is-a-tsunami&catid=1340&Itemid=2056

Uslu, B. U., Admire, A. R., & Dengler, L. A. (2013). Investigating effects of model resolution on computing tsunami currents in Northern California. *International Tsunami Symposium (ITS)*, 122.

Wei, Y., Bernard, E. N., Tang, L., Weiss, R., Titov, V. V., Moore, C., … Kânoğlu, U. (2008). Real-time experimental forecast of the Peruvian tsunami of August 2007 for U.S. coastlines. *Geophysical Research Letters*, *35*(4), L04609. https://doi.org/10.1029/2007GL032250

Yalciner, A. C., Kuran, U., Akyarli, A., & Imamura, F. (1995). An Investigation on the Propagation of Tsunamis in the Aegean Sea by Mathematical Modeling. In Y. Tsuchiya & N. Shuto (Eds.), *Tsunami: Progress in Prediction, Disaster Prevention and Warning* (pp. 55–70). https://doi.org/10.1007/978-94-015-8565-1_4

Yalciner, A., Zaytsev, A., Aytore, B., Insel, I., Heidarzadeh, M., Kian, R., & Imamura,

F. (2014). A Possible Submarine Landslide and Associated Tsunami at the Northwest Nile Delta, Mediterranean Sea. *Oceanography*, *27*(2), 68–75. https://doi.org/10.5670/oceanog.2014.41

Yalciner, Ahmet C., & Pelinovsky, E. N. (2007). A short cut numerical method for determination of periods of free oscillations for basins with irregular geometry and bathymetry. *Ocean Engineering*, *34*(5–6), 747–757. https://doi.org/10.1016/j.oceaneng.2006.05.016

Yalçıner, A. C., Alpar, B., Altınok, Y., Ozbay, I., & Imamura, F. (2002). Tsunamis in the Sea of Marmara: Historical Documents for the Past, Models for Future. *Marine Geology*, *190*, 445–463.

Yalçıner, A. C., Annunziato, A., Papadopoulos, G. A., Dogan, G. G., Guler, H. G., Sozdinler, C. O., … Synolakis, C. (2017). *Post Tsunami Field Survey Report*.

Yalçıner, A. C., Özer, C., Karakuş, H., Zaytsev, A., & Guler, I. (2010). Evaluation of Coastal Risk at Selected Sites against Eastern Mediterranean Tsunamis. *32nd International Conference on Coastal Engineering (ICCE 2010)*. Shanghai, China.

Yalçıner, A. C., Pelinovsky, E., Synolakis, C. E., & Okal, E. A. S. (2003). Submarine Landslides and Tsunamis. In A. C. Yalçıner, E. Pelinovsky, C. E. Synolakis, & E. A. S. Okal (Eds.), *NATO SCIENCE SERIES* (p. 329). Netherlands: Kluwer Academic Publishers.

Yalçıner, A. C., Pelinovsky, E., Talipova, T., Kurkin, A., Kozelkov, A., & Zaytsev, A. (2004). Tsunamis in the Black Sea: Comparison of the historical, instrumental, and numerical data. *Journal of Geophysical Research*, *109*(C12), C12023. https://doi.org/10.1029/2003JC002113

Yalçıner, A. C., Synolakis, C. E., Alpar, B., Borrero, J. C., Altınok, Y., Imamura, F., … Kanoglu, U. (2001). Field Surveys and Modeling 1999 Izmit Tsunami. *International Tsunami Symposium ITS 2001*, 557–563. Seattle, Washington.

Yalçıner, A. C., Synolakis, C. E., González, M., & Kanoglu, U. (2007). *Joint Workshp on Improvements of Tsunami Models, Inundation Map and Test Sites of EU TRANSFER Project*. June 11-14, Fethiye, Turkey.

Yanenko, N. N. (1971). *The Method of Fractional Steps* (M. Holt, Ed.). https://doi.org/10.1007/978-3-642-65108-3

Yılmaz, H., & Erol, E. (2015). Yatlarda Yapısal Üretim Malzemelerinin Tekne Performansına ve Maliyetine Etkisinin İncelenmesi. *3rd International Symposium on Innovative Technologies in Engineering and Science (ISITES2015)*. Valencia - Spain.

Zahibo, N., Pelinovsky, E., Yalçıner, A. C., Kurkin, A., Kozelkov, A., & Zaytsev, A. (2003). Modeling the 1867 Virgin Island Tsunami. *Natural Hazards and Earth*

System Science, 367–376.

Zaytsev, A., Kostenko, I., Kurkin, A., Pelinovsky, E., & Yalçıner, A. C. (2016). The depth effect of earthquakes on tsunami heights in the Sea of Okhotsk. *Turkish Journal of Earth Science, 25,* 289–299. https://doi.org/10.3906/yer-1509-6

Zaytsev, A., Yalçıner, A. C., Chernov, A., Pelinovsky, E., & Kurkin, A. (2016). NAMI DANCE Manual. Retrieved July 30, 2019, from Tsunami Simulation/Visualization Code NAMI DANCE versions 5.0 website: http://namidance.ce.metu.edu.tr/

Zaytsev, A., Yalçıner, A. C., Pelinovsky, E., Kurkin, A., Özer, C., Insel, I., … Özyurt, G. (2008). Tsunamis in Eastern Mediterranean, Histories, Possibilities and Realities. *7th International Conference on Coastal and Port Engineering in Developing Countries,*. Dubai, UAE.

APPENDICES

A. Google Earth Images of Gumbet Bay on Various Days

Figure 0.1. Google Earth image of the berthing places in Gumbet Bay at 12/05/2017

Figure 0.2. Google Earth image of the berthing places in Gumbet Bay at 14/05/2017

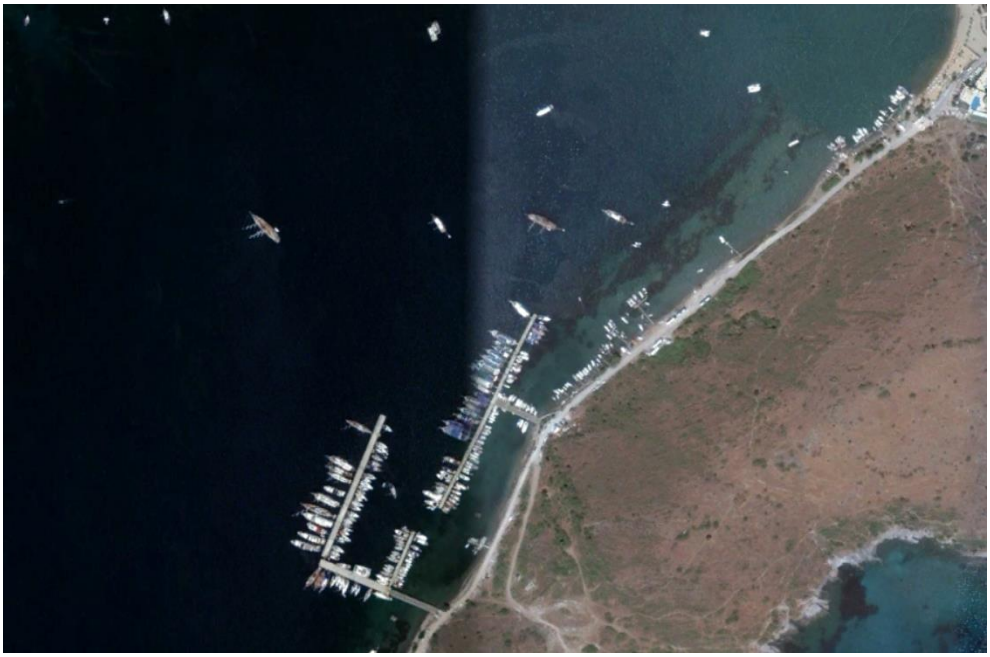

Figure 0.3. Google Earth image of the berthing places in Gumbet Bay at 20/06/2017

Figure 0.4. Google Earth image of the berthing places in Gumbet Bay at 26/06/2017

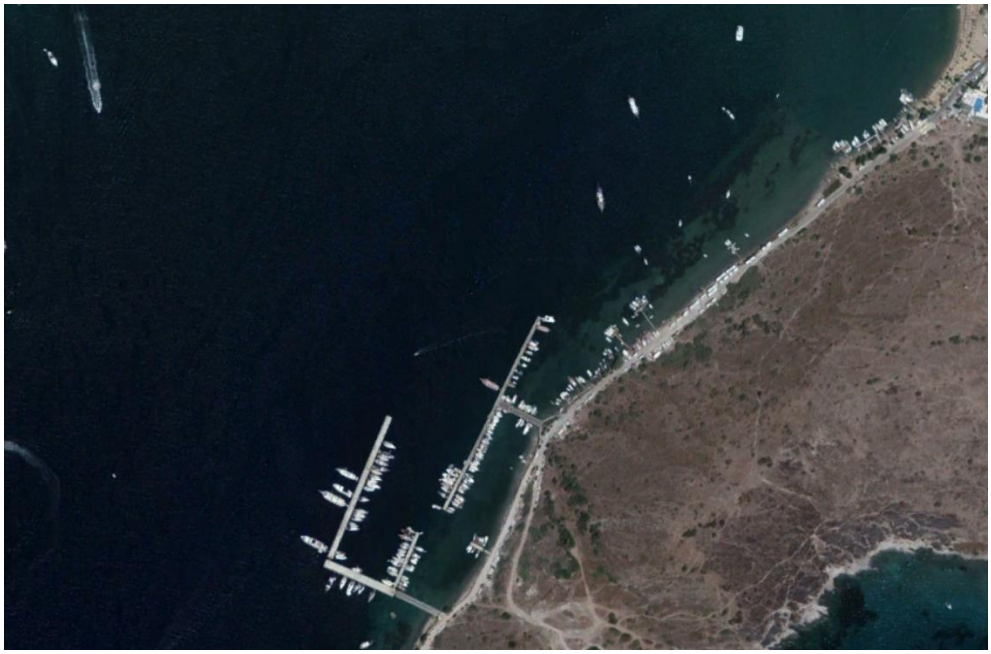

Figure 0.5. Google Earth image of the berthing places in Gumbet Bay at 13/08/2017

Figure 0.6. Google Earth image of the berthing places in Gumbet Bay at 21/09/2018

Figure 0.7. Google Earth image of the berthing places in Gumbet Bay at 13/11/2018